Structural Stiffness Gradient along a Single Nanofiber and Associated Single Cell Response

Sean Meehan

Thesis submitted to the faculty of the Virginia Polytechnic Institute and State University in partial fulfillment of the requirements for the degree of

Master of Science
In
Mechanical Engineering

Amrinder S. Nain, Chair
Bahareh Behkam
Mark R. Paul

May 8, 2013
Blacksburg, Virginia

Abstract

Cell-substrate interactions are important to study for development of accurate *in vitro* research platforms. Recently it has been demonstrated that physical microenvironment of cells directly affects cellular motility and cytoskeletal arrangement. Specifically, previous studies have explored the role of material stiffness (Young's modulus: N/m^2) on cell behavior including attachment, spreading, migration, cytoskeleton arrangement (stress fiber and focal adhesion distribution) and differentiation.

In this study using our recently described non-electrospinning fiber manufacturing platform, customized scaffolds of suspended nanofibers are developed to study single cell behavior in a tunable structural stiffness (N/m) environment. Suspended fibers of three different diameters (400, 700 and 1200 nm) are deposited in aligned configurations in two lengths of 1 and 2 mm using the previously described STEP (Spinneret based Tunable Engineered Parameters) platform. These fibers present a gradient of structural stiffness to the cells at constant material stiffness. Single cells attached to fibers are constrained to move along the fiber axis and with increase in structural stiffness are observed to spread to longer lengths, put out longer focal adhesions, have elongated nucleus with decreased migration rates. Furthermore, more than 60% of cell population is observed to migrate from areas of low to high structural stiffness. Additionally dividing cells are observed to round up and daughter cells are observed to migrate away from each other after division. Interestingly, dividing rounded cells are found to be anchored to the fibers through thin protrusions emanating from the focal adhesion sites.

These results indicate a substrate stiffness sensing mechanism that goes beyond the traditionally accepted modulus sensing that cells have been shown to respond to previously.

From this work, the importance of structural stiffness in cellular mechanosensing at the single cell-nanofiber scaled warrants consideration of the above factors in accurate design of scaffolds in future.

Table of Contents

List of Figures

List of Tables

List of Equations

List of Abbreviations

µl	Microliter
µm	Micrometer
AFM	Atomic Force Microscope
BSA	Bovine Serum Albumin
cm	Centimeter
DC	Direct Current
DRIE	Deep Reactive Ion Etching
ECM	Extracellular Matrix
FA	Focal Adhesion
ml	Milliliter
mm	Millimeter
Mw	Molecular Weight
nN	Nano-newton
NSI	Nuclear Shape Index
PBS	Phosphate Buffered Saline
PDMS	Polydimethysiloxane
PS	Polystyrene
STEP	Spinneret Based Tunable Engineered Parameters

Chapter One: Introduction

1.1. The Importance of Understanding Cell Substrate Interactions

Cell-substrate interactions are important to almost every biological process, including wound healing, stem cell differentiation, and immune response. Each of these processes is dependent on cellular migration and cytoskeletal adaptation to different physical and chemical environments, which take cues from the cell's interaction with the extracellular matrix (ECM) [1,2]. Without the ability to sense and respond to the surrounding chemical and physical environment, these processes would not be possible. Therefore, it is of paramount importance to understand these interactions. As researchers are able to understand the principles behind the base level of cell substrate interaction, the application of these principles allow for improvement of subsequent studies as well as informed design of products that exist to benefit from normal cellular interaction, such as scaffolds designed to replace damaged bone tissue or bandages designed to accelerate healing.

1.1.1 The Role of the ECM

The ECM is a non-cellular construct that is present throughout the whole body and provides both a physical construct for cells to attach to as well as allows for chemical and physical cues to be passed between the single cell and neighboring cells [3,4]. The properties of the ECM are highly tissue specific and these properties, such as pore size and density, chemical composition, and topology serve to provide cues to the cells in order to direct cell behaviors including attachment, spreading, proliferation, migration and differentiation [5,6].

The ECM is constantly being modified and rebuilt by cells as they move around it and abnormal cells are known to have different ECM compared to normal counterparts . Multiple studies have shown that when abnormal cells are in contact with ECM, the properties of that area of the ECM can be significantly altered [7]. This effect is well characterized in the case of cancerous cells, where the presence of tumors has been linked to a cascade of changes in both the physical and chemical microenvironment that both enhance the tumor survival, thus allowing for further microarchitectural changes [8,9], and facilitates cancer metastasis, the leading cause of death in most cancer types [8,10,11]. Understanding the interactions that occur between the ECM and cells, especially in the context of stiffness is incredibly important to understanding cellular behavior in both normal and abnormal cells.

1.2. The Cellular Environment

Cellular behavior is highly reliant on the immediate environment surrounding the cell. Cells probe their environment through ECM interaction with their focal adhesions, responding to both physical and chemical cues received from the immediate area [12]. The environmental cues that cells respond to can be separated into two categories: chemical and physical cues. While there has been extensive research exploring the roles of various chemical interactions between cells and the environment, the effects of the physical environment on cellular behavior has only been studied recently [13]. New insights into these interactions have provided a deeper understanding on how cells sense and respond to the changes to their immediate physical environment.

1.3. Principles behind Cellular Migration

Cellular motility is a critical component in many biophysical processes that are necessary to life, including wound healing, tissue development, and immune response [14–16]. Therefore, understanding the specific actions that facilitate cell migration and the parameters that influence it is of utmost importance.

Cellular migration is a dynamic process involving many molecular components that are still being identified currently. The basic cascade of actions that drive migration can be broken up into five major events: Polarization, membrane extension, adhesion formation, cell body movement, and rear adhesion release [17,18]. Each of these events relies on a complicated combination of spatial and temporal cues from ECM resulting in cell migration.

Polarization is the first step in successful migration. Cells rearrange their cytoskeleton in order to translate forces generated within the cell body to achieve total cell body migration. This action usually begins with a change in actin stress fiber bundle distribution towards the front of the cell, followed by redistribution of microtubules, several receptor types, and adhesion molecules that allow for environmental sensing and membrane protrusion at the leading edge of the cell [19–21]. Polarization, while not necessarily dependent on the cellular environment, responds to a wide range of both chemical and physical stimuli. When cells are polarized, the next step in migration is membrane extension of the leading edge. This is accomplished by two separate but similar structures, lamellipodia and filopodia. Both of these are actin based protrusion organelles that drive migration, but they differ in both their actin polymerization characteristics and physical structure. Lamellipodia consist of a dense network of highly branched actin filaments and are temporally stable, while filopodia are thin, hair-like extensions

3

that are comprised of bundled parallel actin fiber bundles. Filopodia are much more temporally transient and can protrude both in the direction of lamellipodia extension or orthogonally [22,23]. Filopodia are also considered to be important for probing of the microenvironment as well as for mechanotransductive force sensing, which dictate the direction of lamellipodia formation [24]. When filopodia and then lamellipodia form at the leading edge of the cell, adhesions are then formed at the tip of the lamellipodia. Focal adhesions serve as both binding structures for chemical and physical receptors and also serve as the traction force transmitting structures at the cell-substrate interface [24–27]. Because of their importance to these various substrate interactive behaviors, focal adhesion formation and organization have been shown to be predictive of cellular migration dynamics [28]. After sufficient focal adhesion formation, cell body translation is accomplished by contraction of the acto-myosin cytoskeleton. During this action, the cell body translates over the focal adhesions that have been established, resulting in retrograde flow of actin and focal adhesions [29,30]. During this flow, the rear adhesions are eventually released, and the cascade cycles, thus, providing continuous migration.

The actions that cells perform during migration are important to understand, because throughout the whole process, complicated sensing of the chemical and physical environment is occurring, which dictates migration dynamics like cell speed, persistence, and direction. Thus it is important to develop biological assays which allow for systematic investigation of cell migration in varying mechanistic and chemical environment.

1.4. Substrate Dimensionality and Microarchitecture

One of the most widely studied physical characteristics of the cellular environment is the substrate dimensionality. The majority of information that exists regarding cell-substrate

interactions was gathered using two dimensional high stiffness (glass) and low stiffness (gel) substrates [28,31–34]. While these studies have provided a wealth of information regarding cellular behavior, it has come to light recently that two dimensional substrates fall short in modeling the *in vivo* cellular environment, where cells migrate on and through the fibrillar ECM [35,36]. Therefore, many recent studies have moved towards using three dimensional substrates, usually collagen gels, to study cellular migration in conditions that mimic the *in vivo* environment.

The study of dimensionality on cell behavior has yielded many insights into how cells respond to the physical parameters of their substrate in conditions other than flat. The majority of these studies have been performed in collagen gels, where cells are either allowed to infiltrate into the gel or are inserted by injection or by depositing gel on top of cultured cells. These studies have shown that there is a considerable difference in cellular behavior in two dimensional substrates compared to three dimensional [36–38]. However, moving towards more biologically relevant substrates has increased the complexity of capturing cell substrate interactions. The most commonly used substrates used for studies of this type are collagen gels, which have been shown to have a complex microarchitecture with varying pore size and fibril diameter. Thus, the use of fibrous constructs and collagen gels adds an extra layer of dimensionality inherent in the complex microarchitecture that make up these substrate types. This in and of itself is not a problem, as the bulk properties of these constructs can still be controlled and characterized. However, the importance of the microarchitecture of scaffolds like these has recently come into light in several studies. It has been shown in various studies that the location specific pore size,

collagen fibril modulus, gel thickness, and other parameters of the microarchitecture have specific effects on cellular behavior regardless of the bulk properties of the gel. [31,39].

1.5. Cellular Mechanosensing

As the importance of the physical cellular environment has become increasingly apparent, investigation of cellular response to changing Young's modulus (material stiffness) has been an area of intense study. It has been found previously that the modulus of the ECM is highly tissue specific, ranging from tens of Pa to GPa range [40], and that cells rely on this stiffness to direct their behavior, especially for differentiation and migration [32,41–45]. Several studies have characterized this link, indicating that stem cells will preferentially differentiate into bone, muscle, or nerve cells in response to changes in substrate stiffness [32,46]. Interestingly, it has also been shown that this relationship holds for both two and three dimensional substrates, but rely on different mechanosensing pathways respectively [47]. Additionally, it has been shown that there is a strong relationship between migration speed and substrate modulus, whereby cells tend to migrate more slowly on stiffer substrates and preferentially migrate in the direction of high stiffness [48]. All of these results indicate that cells are constantly sensing and responding to their physical environment, modulating their behavior and cytoskeletal arrangement based on substrate modulus. Understanding these sensing mechanisms allows for a detailed investigation of the sensing pathways that control cell behavior, allowing for more accurate representation of biological tissues *in vitro* for research purposes as well as for informed design of products like bandages and implants that can take advantage of these behaviors.

Chapter Two: Statement of Problem

A complete understanding of the interaction between cells and their immediate environment is immensely important to allow for informed experimental design and design of biomechanical devices. While the chemical interactions that govern cellular behaviors are reasonably well characterized, there has been growing interest in how physical interaction between cells and their substrates affect cellular behavior. In order to understand these physical interactions, the effects of changing substrate material stiffness (Young's modulus (N/m^2)) has been explored and found to affect many cellular behaviors, including cell motility and cytoskeletal arrangement. However, it has been shown in many cases that the properties of the physical microenvironment can have important and sometimes very different effects on cellular behavior than the properties of the macro bulk environment, indicating a level of environmental sensing that is more complex than previously thought.

This study aims to test the cellular interaction with structural stiffness using a unique substrate type. It is expected that cells that are attached to a single suspended nanofiber will sense and respond to the local structural stiffness by modulating their cytoskeletal arrangement, leading to changes in migration dynamics. This response is expected to occur in the absence of any change of material modulus, providing insight into a cellular mechanosensing mechanism that goes beyond the traditionally accepted understanding of sensing material modulus.

Through this study it has been shown that cells do in fact respond to changes in structural stiffness (N/m) along a single suspended nanofiber without any change in bulk Young's modulus. This indicates that there is a degree of localized substrate stiffness sensing present that

goes beyond the traditionally accepted bulk sensing, and that migrating cells are manipulating their substrate (the fibers) in a way that allows for sensing of structural stiffness. This finding has important implications in the general understanding of cellular mechanosensing as well as for informed experimental and device design in the future.

Chapter Three: Materials and Methods

3.1. Scaffold Design and Fabrication

Several scaffold types were created to provide control over the mechanical environment presented to single cells. Single PS nanofibers were deposited over all substrate types using the STEP method. The STEP method allows for control over the fiber diameter, alignment, and spacing that was necessary for providing cells with a repeatable structural stiffness gradient. A brief review of the STEP process and its capabilities can be found in Section 3.3.3. The use of suspended nanofibers allows for a controllable structural stiffness gradient used to observe cellular response.

3.2. Micropillar Substrates

Micropillars were utilized as raised platforms for fiber deposition in early substrate designs. The design of these substrates went through several improvements throughout the course of the project.

3.2.1 Punched Micropillars: Substrate Fabrication

Early substrates were produced by attaching hand-punched millimeter scale PDMS pillars to glass coverslips. Pillars were made using a tissue core sample punch (Harris Uni-Core) to punch cylindrical pillars out of large scale blocks of cured PDMS. Handmade pillars were made in sizes of 1 mm, 0.75 mm, and 0.5 mm. Pillars were collected from the punch, and later adhered to glass substrates using two part epoxy (Devcon) or uncured PDMS. After adhesive was fully cured, fibers were deposited over the substrate using the STEP method explained in section 3.3.3.

3.2.2 Molded Pillars: SU-8 Soft Lithography

Soft lithography was utilized to produce molds used in the creation of films with attached micropillars. Traditional SU-8 Lithography was used to create large scale (50µm) pillars. SU-8 molds were created as follows.

Silicon wafers (University Wafer Inc.) were placed onto a photoresist spinner and spun for 1 minute at 1000 rpm, during which cleaning was performed by applying acetone followed by isopropyl alcohol, and finally with distilled water. Wafers were then baked at 65°C for five minutes to ensure a dry surface. After cooling, wafers were placed back into the photoresist spinner, coated with ≈5 ml. of SU-8 2025 photoresist (Microchem Inc.), and spun at 500 rpm with an acceleration of 100 rpm/sec for 8 seconds, and 1750 rpm with an acceleration of 300 rpm/sec for 30 seconds. This deposited a coating of approximately 40 µm thickness. Edge bead removal was then performed by spinning at 5000 rpm for 10 seconds.

A soft bake were performed at 65°C for 3 minutes, and then 95°C for 6 minutes. To ensure that all solvent was removed from the resist, wafers were removed from the heat source and allowed to cool, then heated back to 95°C. If the photoresist did not wrinkle when heated, the solvent removal was complete. After baking, wafers were exposed at 40 mW/s for 40 seconds using an MA-6 Mask Aligner to set photoresist. After exposure, a post exposure bake was performed at 65°C for 1 minute, and then 95°C for 6 minutes. After baking, a latent image of the mask pattern could be seen. An example drawing on the mask pattern uses to expose photoresist and the resulting micropillar pattern can be seen in Figure 1.
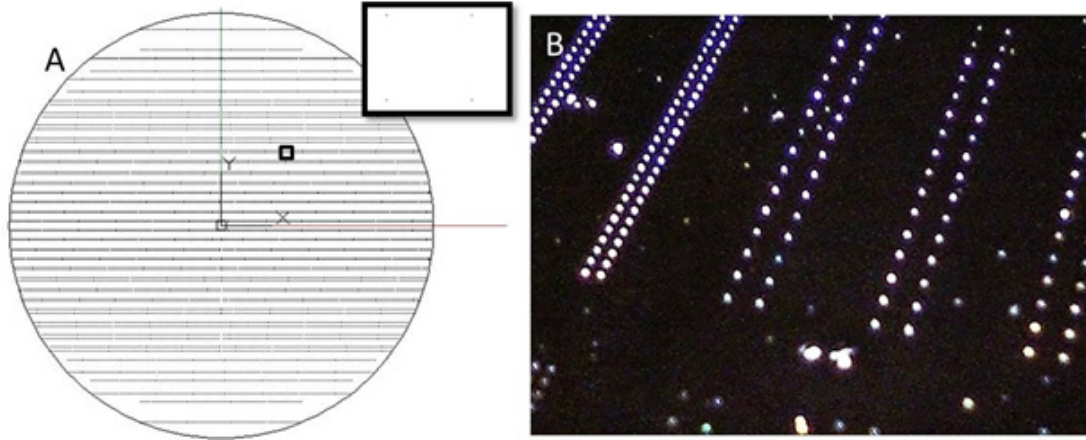
Figure 1. A) Drawing of mask file used to create microwell array. Inset shows typical hole pattern. B) Image of wafer with microwells. Microwells are filled with PDMS to create micropillars.

After the post exposure bake, wafers were developed in SU-8 Developer for five to ten minutes. Developer was agitated by hand until all unexposed photoresist was removed.

3.2.3 Molded Pillars: Reactive Ion Etching

In order to reliably create micropillar molds with small, high aspect ratio features, Deep Reactive Ion Etching (Alcatel) was used. AZ 4620 photoresist was used to coat wafers to provide resistance to the etching process. The process for AZ 4620 lithography is as follows.

Wafers are cleaned as described in Section 3.2.2. AZ 4620 was deposited onto the wafer, and then wafers were spun at 2000 rpm for 40 seconds at an acceleration of 425 rpm/s. Wafers are soft baked at 95°C for 12 minutes, exposed at 40 mW/s for 1 minute, post baked at 95°C for 20 minutes, and then developed for 1.5 minutes with AZ 4620 Developer.

After features were outlined with AZ 4620, deep reactive ion etching was performed using an Alcatel AMS 100 DRIE machine. Etching was done using normal silicon etching

techniques pre-programmed into the AMS 100. Etching was performed for 30 minutes to create 100 μm height features.

3.2.4 Molded Pillars: Pillar Fabrication

After proof of concept experiments with hand placing pillars, soft lithography was utilized to create molds. Micropillars were produced in several sizes and configurations throughout this project. Soft lithography was used to create silicon wafers with micro scale wells placed in various configurations, which were coated in polydimethysiloxane (Sylgard 184, Dow Corning) to create films with micron scale pillars on them. Wells of fifty and ten micron diameters were used. The procedure for passivation of wafers and PDMS molding is as follows.

SYLGard 184 PDMS was mixed according to manufacturer's instructions at a ten to one ratio by weight of base to catalyst. PDMS was mixed using a disposable inoculating loop until it was well mixed with air bubbles incorporated into mix. PDMS solution was then degassed at 35 mm H_2O for at least twenty minutes, until all air bubbles left the solution. While PDMS was degassing, wafers were coated with chlorotrimethylsilane (Sigma-Aldrich) by placing wafers into a Nalgene Vacuum Desiccator with a petri dish with 5 ml of chlorotrimethylsilane and removing all air. Wafers were left in desiccator for 30 minutes, then removed and PDMS was then poured over silicon molds immediately. This facilitated easy removal of PDMS films with minimal pillar breakage. Silicon molds were baked at 60°C for 45 minutes, or until PDMS was totally cured. PDMS molds were then peeled by hand from molds, resulting in a PDMS film with attached micron scale pillars. PDMS films were cut into usable pieces using a razorblade. Film pieces were attached to No. 0 glass coverslips using uncured PDMS as an adhesive, and baked once again at 60°C until cured.

3.2.5 Block Substrate Fabrication

Because using micropillars to create revised platforms for nanofibers caused difficulties in fiber deposition, an alternative substrate type was designed. To create substrates that allowed for easy fiber deposition of suspended fibers, PDMS blocks were affixed to glass coverslips. First, number 0 glass coverslips (Fisher Scientific) were cut into four by twenty mm rectangles using a carbide scribe (McMaster-Carr) to score the coverslips, and then pressure was applied by hand to break them along the score lines. Then, PDMS blocks of two mm thickness were cut using a razorblade into one by ten mm pieces. Uncured PDMS was applied to the glass cover slip pieces, and PDMS blocks were affixed to the coverslips using the uncured PDMS. In order to create a permanent junction, samples were then cured in a vacuum oven at 60C for at least 45 minutes, or left to cure at room temperature overnight.

3.3. Fiber Deposition

Fibers were deposited on the previously mentioned substrates using two methods. The first method, used with micropillar arrays, was a hand deposition method. Eventually, testing was shifted to a more conventional STEP spinning method that allowed for greater control over fiber properties, increased consistency between samples, and higher throughput.

3.3.1 Polymer Solution Preparation

Polymer solutions were prepared by incorporating polystyrene (Mw: 2,257,000 g.mol^{-1}) into Xylene (Sigma-Aldrich) in three different concentration: 5%, 7%, and 13% w/w.

3.3.2 Hand Deposition

Depositing fibers by hand allowed for control over the fiber boundary placement to specific micron scale pillars, but was not conducive to providing fibers with controllable diameter. Hand deposition was accomplished by dipping a 100 μm diameter probe tip in PS polymer solution and then bringing the droplet of solution clinging to the probe tip in contact with a substrate. Moving the probe tip along the substrate allowed for drawing of single nanofibers.

3.3.3 STEP Method

The STEP method of nanofiber deposition can be reviewed in detail in several previous works [49,50]. Polymer solutions of PS dissolved in xylene were brought into contact with rotating substrates. When the polymer solution is brought into contact with the rotating substrate, molecular entanglement allows for drawing of a nanoscale PS fiber. When fibers begin to deposit, the substrate is moved laterally, with the movement speed dictating fiber spacing. By controlling the polymer solution parameters and substrate motion, precise control over fiber diameter, lateral spacing, and alignment is possible. This control allows for deposition of similar fibers to provide a repeatable structural stiffness gradient.

3.4. Theoretical Fiber Structural Stiffness

In addition to AFM characterization of fiber structural stiffness described in Appendix A, a theoretical stiffness model that describes the relationship between distance from the fixed fiber ends and fiber structural stiffness was established. This relationship was described using simple

Euler-Bernoulli beam mechanics. Fibers were modeled as a simply supported beam subject to bending at various points along their length, which is an analog to the forces placed on fibers by cell mechanosensing as shown in Figure 2.
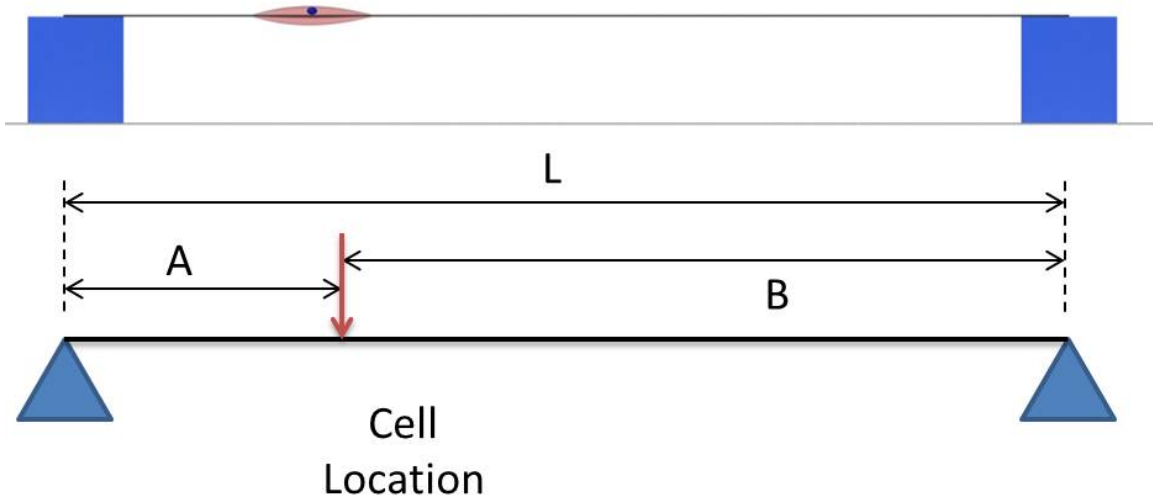
Figure 2. Theoretical model used to estimate structural stiffness. The force applied to the fiber is analogous to the mechanosensing mechanism employed by the migrating cell.

The relationship that was used to characterize theoretical stiffness is identical to the equivalent spring constant of a simply supported beam, seen below in Equation 1.

$$k_{Structural} = \frac{3EIL}{A^2 B^2}$$
Equation 1

Where E is the material Young's modulus (3 GPa for PS), I is the moment of inertia for the fiber, L is the fiber length, and A and B describe the position of the cell. This relationship was used for all characterization of cellular behavior.

3.5. Substrate Preparation

Before using substrates for experiments, they were placed in glass-bottom six well plates using vacuum grease to ensure that they did not float when media was added. Substrates were then soaked in 70% ethanol for at least five minutes to sterilize, and then washed with PBS twice. Fibers were then coated with 2μg/ml fibronectin and kept in an incubator at 37°C for at least 8 hours. After functionalization, fibers were ready to have cells cultured on them.

3.6. In Vitro Cell Studies

To understand the effects of structural stiffness on cellular migration and cytoskeletal arrangement, in vitro studies were conducted using C2C12 mouse myoblast cells. C2C12 are myoblast cell line capable of differentiation along both osteogenic and myogenic pathways. They have been previously used for exploration of mechanistic pathways and associated protein expression because of their high contractile forces and adhesion dynamics. They have been used within a variety of polymer substrate studies to explore the effects of patterning and substrate stiffness on cellular behavior, and thus present opportunities for comparison [41,52–55].

3.6.1 Cell Culture

Standard cell culture protocols were followed in all instances. C2C12 mouse myoblasts were obtained from ATCC and maintained in DMEM supplemented with FBS and antibiotics. Cells were cultured in a standard cell culture incubator at 5% CO_2 and 37°C. Cells were passaged when confluence reached 60-70%, and singular lines were not used past passage 20.

For migration/cytoskeletal arrangement studies, cells were used at a concentration of 20,000 cells/ml, due to low seeding efficiency. Before use, cells in a flask were trypsinized, counted, and the correct amount of cells were added to each scaffold. 1 ml of DMEM containing C2C12 cells was added to each substrate, and after attachment another 1 ml of DMEM without cells was added to each well.

3.6.2 Migration Characterization

Migration speed was characterized using a Zeiss Axiovision Z1 inverted microscope with full incubation enclosure. During time lapse imaging, cells were kept at a constant 5% CO_2 and 37°C. Image positions were set along the entire length of each fiber studied in order to obtain a complete view of cellular interaction with changing structural stiffness. Displacement of the cell body was tracked over each hour of each time lapse video, and migration speed was characterized as the distance between the cellular position at the beginning and end of the hour time period, measured in µm/hr. Cellular position was defined as the distance from the center of the fiber at the beginning of the hour time period for each data point. Direction of migration was recorded in reference to migration either towards or away from the center of the fiber. Cells observed to be undergoing mitotic events or coming into contact with other cells were not taken into account from the point that the event occurred, thus, minimizing the effects of contact inhibition on measured migration speed.

3.6.3 Cellular Persistence Characterization

Cellular persistence is a measure of how directed cell migration is. While persistence measurement normally entails measuring the angle and direction of cellular movement on flat, this measurement is simplified by the physical constraint placed on cells because they are

17

traveling along a single fiber. Cellular persistence was characterized using Equation 2 and Figure 3 demonstrates the measurement method. Persistence was measured as a ratio of the distance between the cell position at the start and end of the measured interval to the actual distance traveled by the cell during the time interval. A persistence of one would correspond to migration in only one direction with no turns, and becomes lower than one with more movement away from the overall direction of travel.

Actual Cell Movement

n

m

l

A ────────────────────────────► B

A - B

Overall Change in Position (A to B)
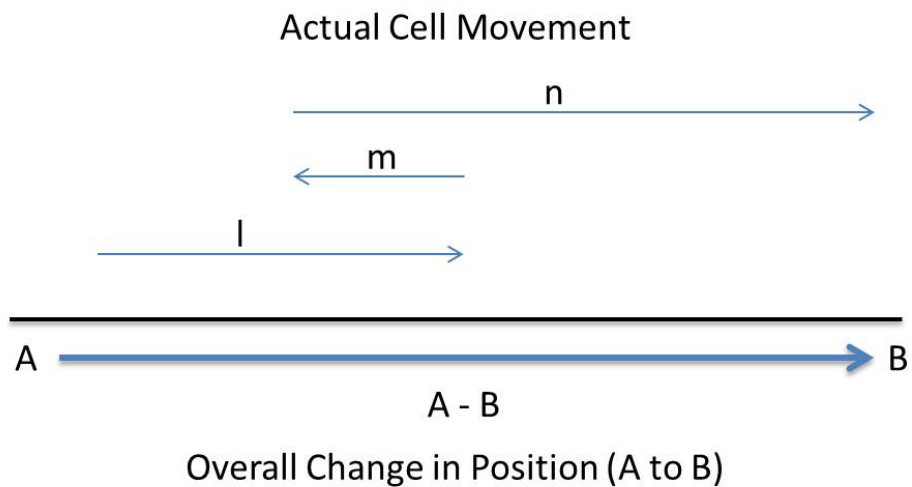
Figure 3. Typical cell movement. Persistence is measured as a ratio of the distance between the starting and ending points of the cell over the measured time interval and the actual distance traveled in that time.

$$Persistence = \frac{|B - A|}{|l + m + n|}$$

Equation 2

3.6.4 Blebbistatin Inhibited Migration

Blebbistatin has been previously shown to disrupt the actin myosin force sensing mechanism, which disrupts a cell's ability to detect physical cues from the substrate and apply traction forces [56–58]. Blebbistatin was used at a concentration of 20 µM, a level previously

18

shown to inhibit the actin myosin complex after 1 hr [30]. Cells were left for 1 hour and time lapse microscopy was then started as described in Section 3.6.2.

3.7. Immunostaining Studies

Immunostaining was used to observe cytoskeletal components important to cell substrate interactions, namely focal adhesions, F-Actin stress fibers, and the nucleus. Characterization of these components was performed by taking fluorescent images at 40x magnification of single cells, as well as mosaic images of the entire length of fibers at 20x for identifying cell location. Measurements of cytoskeletal components were performed using AxioVision software.

3.7.1 Immunostaining Protocol

After migrations studies were complete, cells were fixed in 2 ml of 4% paraformaldehyde for 15 minutes. Cells were then permeabilized using a solution of BSA and Triton X-100 for 15 minutes. Blocking was performed by coating substrates with 10% goat serum blocking buffer (Invitrogen) for 30 minutes. Rabbit anti-paxillin primary antibodies (Invitrogen) were used at a 1:250 dilution ratio along with goat anti-rabbit GFP secondary antibodies (Invitrogen) to image FACs. F-actin stress fibers were stained with rhodamine-conjugated phalloidin (Santa Cruz Biotechnology, CA) diluted 1:100. Nuclei were counterstained with DAPI (Invitrogen) for 5 minutes.

3.7.2 Cytoskeletal Component Measurement

The cytoskeletal components of interest and the methods used to measure them can be seen in both illustrated form and as an actual representative image in Figure 4.
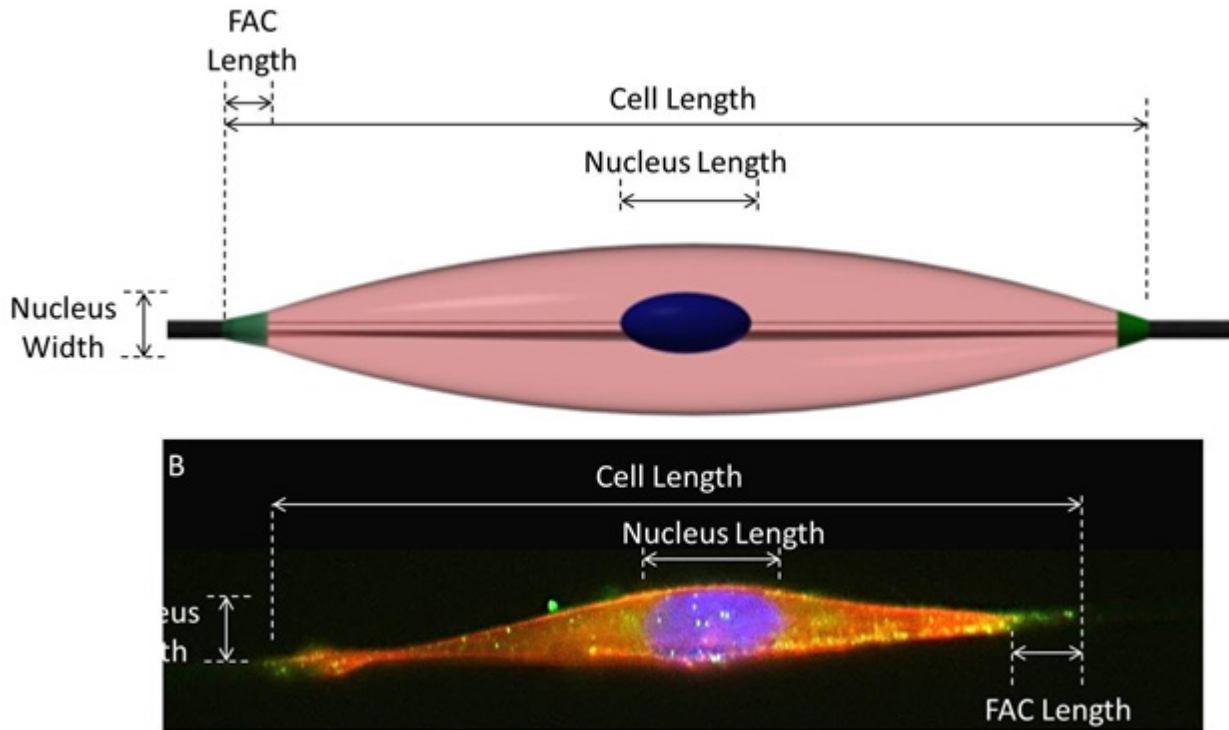
Figure 4. Cytoskeletal parameters of interest shown on A) a diagram and B) a representative image of an immunostained cell on a fiber.

All measurements were performed using AxioVision software. To determine the nuclear shape index, the nucleus length and width were measured using AxioVision software and were then used to analytically find the area and perimeter of the nucleus. Nucleus shape index (NSI) was determined as:

$$NSI = \frac{4\pi\,Area}{Perimeter^2} = \frac{2LW}{L^2 + W^2} \qquad \text{Equation 3}$$

Where L and W correspond to half of the nucleus length and width respectively.

3.8. Statistical Testing

Statistical analysis and graphing were performed using GraphPad software. One way ANOVA testing with Tukey post testing comparing all pairs of data sets was performed, with the results presented here. Standard presentation of statistical significance is used, with * indicating a P value less than or equal to 0.05, ** indicating a P value less than or equal to 0.01, and *** indicating a P value less than or equal to 0.001. All column figures are shown with brackets indicating standard deviation.

Chapter Four: Results

4.1. Scaffold Design and Fabrication

Creation of scaffolds with repeatable properties was integral to providing similar stiffness profiles for cells between experiments. Scaffolds used for data collection were all of the Block Substrate type outlined in section 3.2.5. This was due to the difficulty of depositing single nanofibers onto the center of micropillars. With the block substrate type, nanofibers could be deposited anywhere along the substrate as long as spacing between fibers was large enough to prohibit cells interacting with more than one fiber. Scaffolds were assembled out of glass slides with PDMS blocks affixed to them at a spacing of either one or two mm. A representative drawing of a typical block type scaffold can be seen in Figure 5.
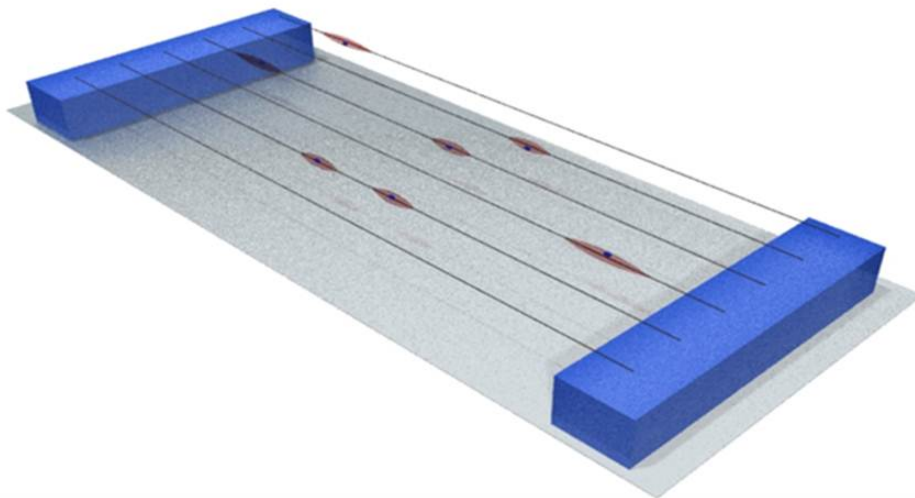
Figure 5. Typical block type substrate with cells attached to single fibers.

4.1.1 Fiber Deposition/Parameter Control

Control on fiber spacing was necessary to both maximize the number of fibers per sample and prohibit cells from interacting with more than one fiber. Fiber spacing was ensured by laterally translating substrates at a fixed speed during fiber deposition. Spacing was later verified both optically and by SEM. Fibers of three diameters (400, 700, and 1200 nm) and two lengths (1 and 2 mm) were used in order to present a large range of structural stiffness values to migrating cells. Two millimeter length fibers of 400 nm diameter provide the lowest structural stiffness range, and overall stiffness range increases with increasing diameter and decreasing length.

4.1.2 Fiber Boundary Fixation

Providing fixed boundaries to fibers was necessary to ensure a repeatable structural stiffness gradient. Before deposition of nanofibers onto either PDMS blocks or micropillars, uncured PDMS was applied by hand to raised constructs using a pipette tip. Fibers were deposited over the coated raised constructs. Deposited fibers sunk into the thin layer of uncured PDMS, and then were allowed to cure overnight at room temperature, to ensure there were no thermal effects on fibers. After curing, selected fibers were broken past the PDMS covered ends to verify that fibers were fixed to the raised constructs. These results were further confirmed with SEM images. Representative images showing the fixed end of a single fiber can be seen in Figure 6.
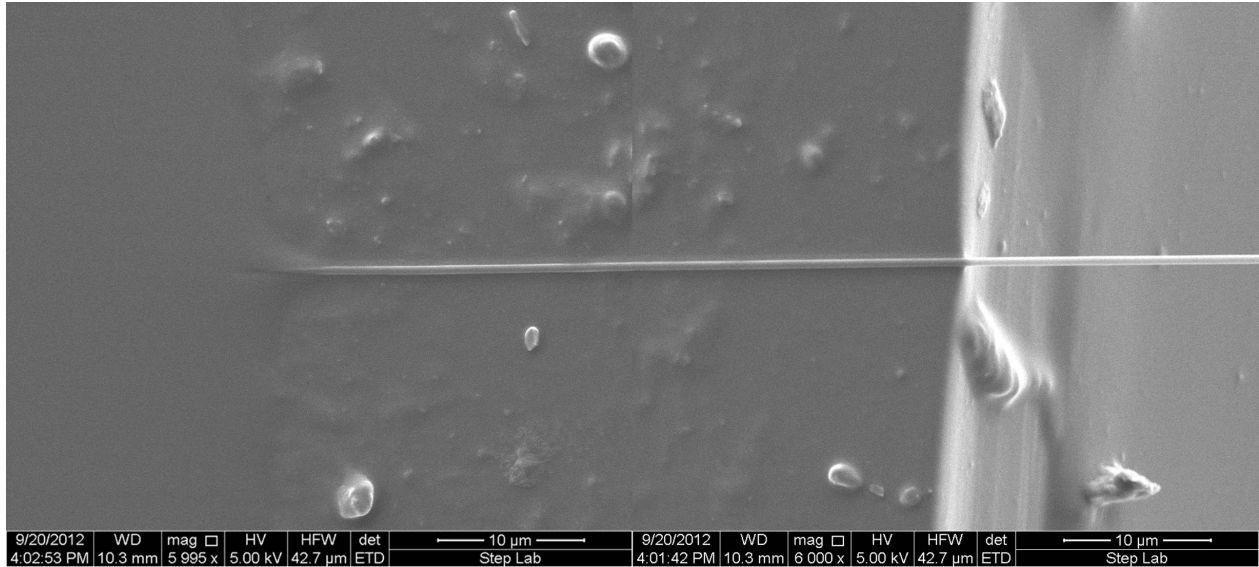
Figure 6. SEM Images showing fixed fiber boundary condition. Mosaic SEM images show the fixed boundary of a single nanofiber

4.2. Fiber Structural Stiffness Characterization

Theoretical stiffness values based on the equivalent bending stiffness shown in Section 3.4 were used in the characterization of cellular behaviors. A representative image showing theoretical stiffness for fibers with a diameter of 700 nm and lengths of 1 and 2 mm can be seen in Figure 7. These stiffness measurements were confirmed using AFM in three point bending mode, as described in Appendix A.
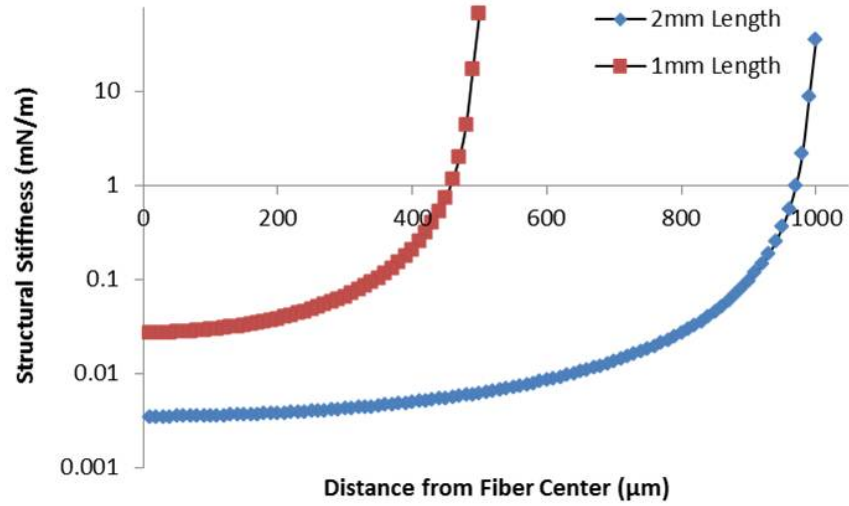
Figure 7. Theoretical structural stiffness gradient along a single nanofiber for 700 nm diameter fibers of 1 and 2 mm length. This relationship is found using simple the simple equivalent stiffness equation. Structural stiffness values are plotted on a logarithmic scale

4.3. Cellular Migration Speed Response to Structural Stiffness

Migration speed of single cells was characterized in response to changes in fiber structural stiffness, and it was found that the speed of migrating cells exhibits an inverse relationship to fiber structural stiffness as shown in Figure 8.
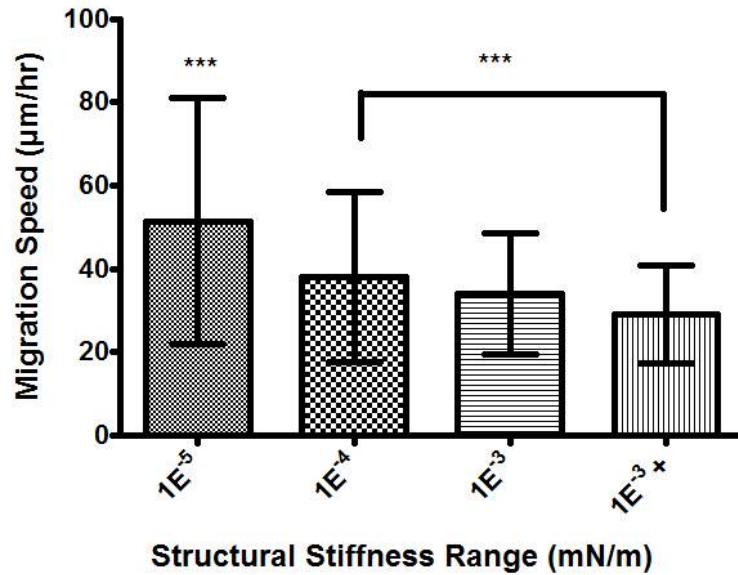
Figure 8. Single cell migration speed response to structural stiffness. Cells migrate slower on areas of higher structural stiffness.

As seen in Figure 8, single cell migration speed responds to structural stiffness noticeably, with cells moving slower on areas of increased structural stiffness. This relationship shows a 22.38 μm/hr decrease in migration speed from the lowest stiffness to the highest stiffness area. The same trend was observed across fibers of all diameters, indicating that the relationship seen is not due to changes in fiber diameter. The scatterplot of this data is shown in Figure 9. However, there are some slight differences in migration speed between the three fiber diameters, which implies that there may also be some relationship between fiber diameter and migration speed.
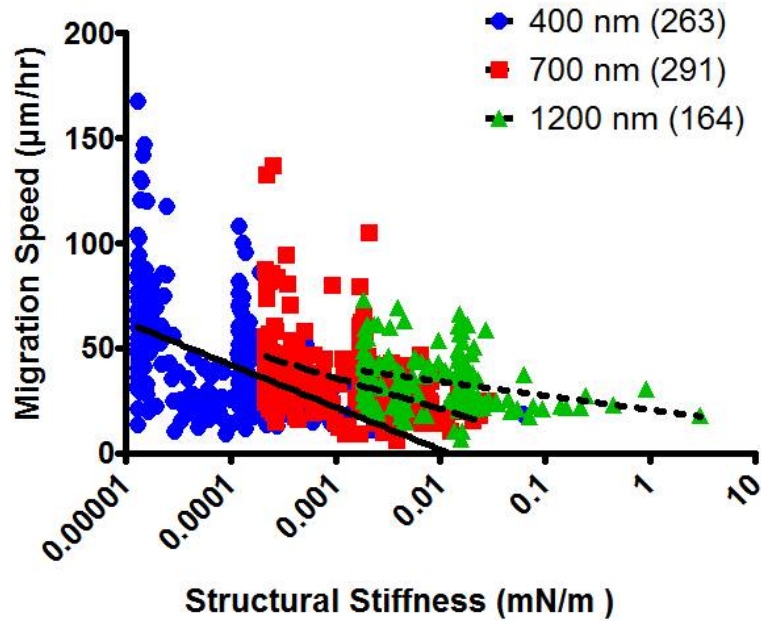
Figure 9. Migration speed response to structural stiffness. The same trend of decreasing migration speed in response to increasing structural stiffness is seen for all fiber diameters

4.4. Cellular Persistence and Directionality

Cellular persistence is a normalized value that serves as a measure to characterize directed cellular migration. Traditionally cells are considered to have persistent motion if on flat substrates if cells show overall migration without deviating from their travel direction more than a certain amount of degrees. However, cells traveling along single nanofibers are restricted to move only along the fiber axis. This requires modifying the definition of persistence for aligned single cell-fiber systems. Persistence in this system is defined by Equation 2, which is further explained in Section 3.6.3.

It was found that cellular persistence was overall very high, with an average value close to 0.8, indicating 80% of cellular migration occurred with no changes in direction. Additionally, there was a slight increase in persistence at high structural stiffness, as seen in Figure 10.
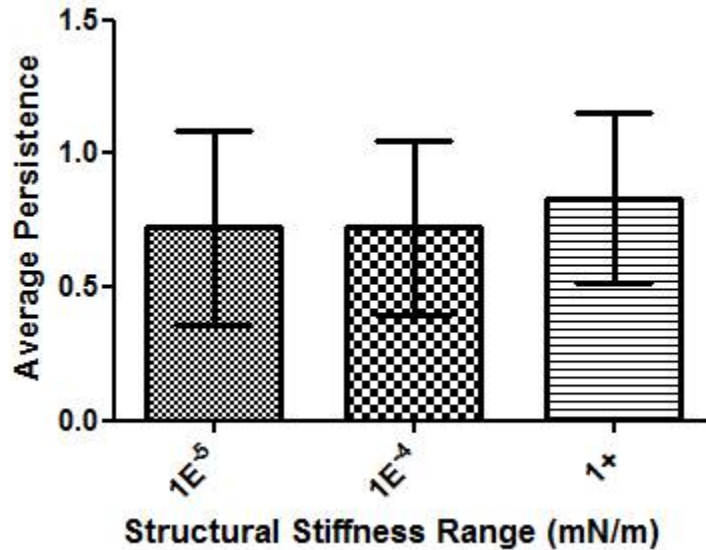
Figure 10. Cellular migration was overall highly persistent, and showed a slight increase at high structural stiffness values.

In addition to migration persistence, migration direction was also recorded. It was shown that cells have a higher tendency to migrate towards areas of higher stiffness (fixed fiber ends), than towards the lower stiffness areas (fiber center), as shown in Figure 11.

These results agree with current studies that indicate that cells will tend to migrate towards areas of higher elastic modulus [48,59]. Additionally, the results shown in here and in section 4.3 indicate that cells are not only migrating towards the areas of higher stiffness in a persistent fashion, but also decreasing their migration speed when they reach the higher structural stiffness area. This mechanism of migration suggests that cells are actively searching

for areas of higher structural stiffness and modulating their migration characteristics to reach those areas.
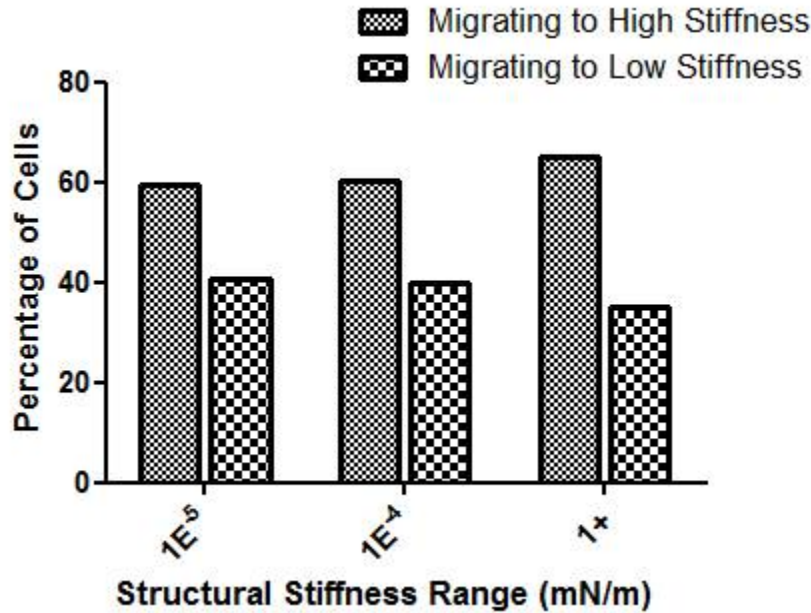
Figure 11. Cellular migration occurred in the direction of higher stiffness a majority of the time at all stiffness values.

4.5. Blebbistatin Treated Cellular Migration

Blebbistatin has previously been shown to inhibit force sensing in cells by disrupting the actin myosin II contractility mechanism that is largely thought to be responsible for force and dimensionality sensing in migrating cells [56,60]. Disrupting this mechanism is known to inhibit the cells ability to modulate migration speed in response to substrate stiffness. To investigate the role of Blebbistatin, experiments were performed on 700 nm diameter fibers with addition of 20 µM blebbistatin to cell culture and measurements were taken 2 hours post Blebbistatin addition.

No discernible trend and no statistical significance between migration speed and structural stiffness was observed as shown in Figure 12.
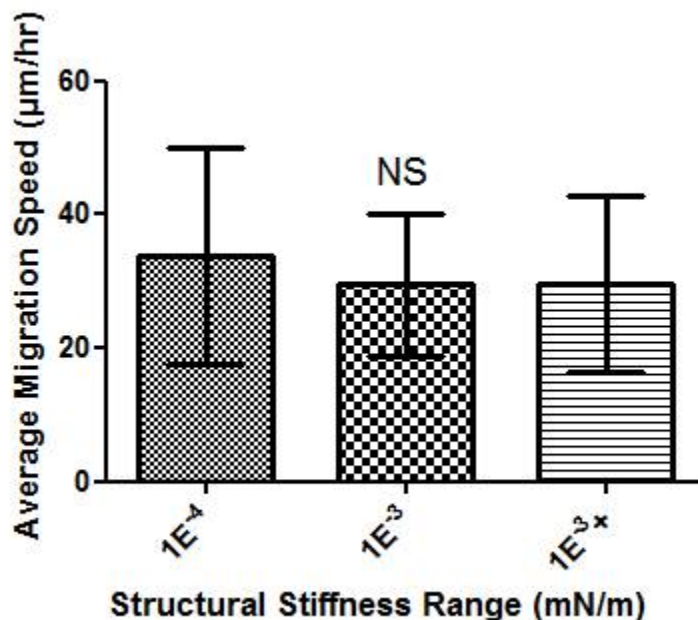
Figure 12. Migration with blebbistatin. Blebbistatin has formerly been shown to inhibit the force sensing mechanism cells use to modulate migration speed in response to substrate stiffness. No significance or discernible trend is present as structural stiffness

4.6. Cytoskeletal Response to Structural Stiffness

As shown in Section 4.3, migration speed shows an inverse relationship to structural stiffness. To further explore this phenomenon, various cytoskeletal components were investigated using immunostaining. A representative stitched mosaic image of the entire length of fiber as well as detailed stained images of several single cells attached at different locations is shown in Figure 13.
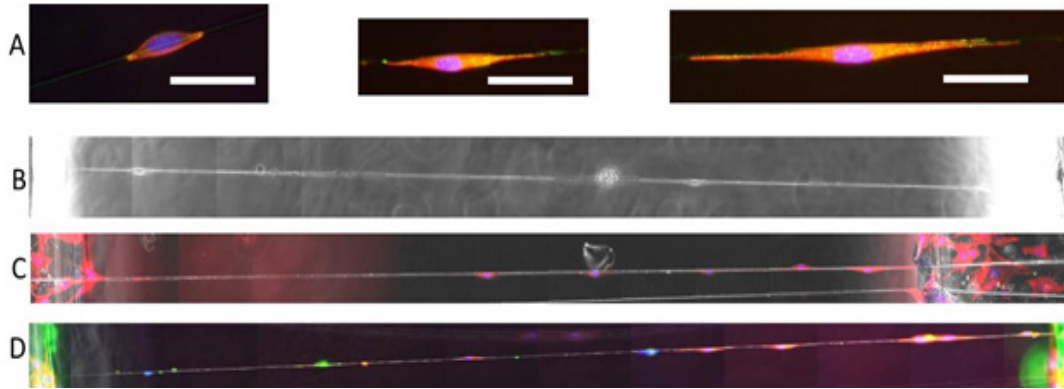
Figure 13. Representative images used to investigate cellular cytoskeletal response to structural stiffness. A) Detail images of several single cells, showing the nucleus (blue), F-Actin stress fibers (red), and focal adhesion clusters (green). B) Phase image of a mosaic showing a single fiber with several cells attached. C) Phase/fluorescent combined image showing phase image as in B as well as F-Actin stress fibers and cell nuclei. D) Fluorescence mosaic image showing all cytoskeletal components of interest. A) Scale bars are 50µm. B,C,D) Scale bars are 100µm.
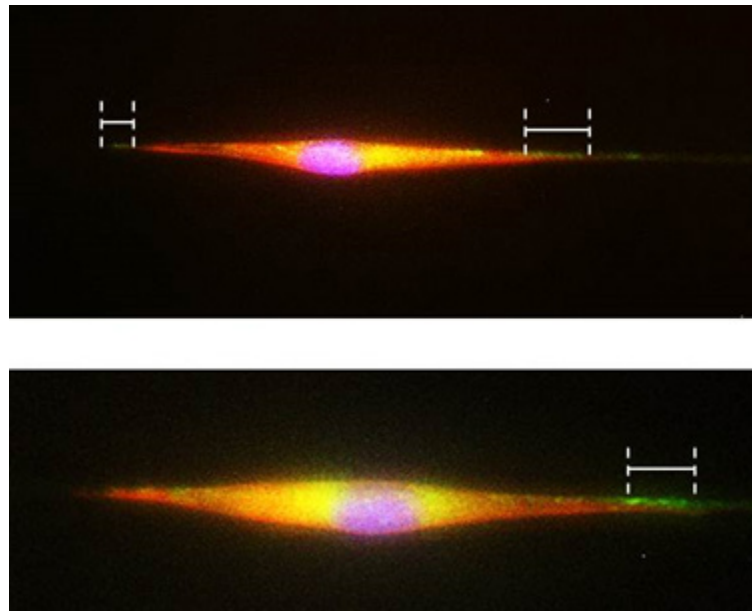
Figure 14. Focal adhesion cluster length illustrated. Focal adhesions can be seen in detail images of two cells. Focal adhesions were not always visible enough to measure on both sides of the cell due to background noise from cells on the glass underneath the fibers.

4.6.1 Focal Adhesion Cluster Length

Paxillin is a cytoplasmic protein that has been shown to localize to focal adhesions and interact with many other structural and signaling proteins. Because of this, the presence of paxillin is a good indicator of mature focal adhesions [61]. Focal adhesions were immunostained for Paxillin and characterized on single fibers. Because cells are limited to spreading over a single nanofiber, focal adhesions were observed to be concentrated at the poles of the cells as shown in Figure 14.

Typically on flat substrates, characterization of focal adhesion area is related to the cell spread. However, for cells attached to suspended nanofibers, the curvature of the fiber is believed to introduce cell wrap around the fiber. This amount of wrapping around fibers by a single cell is extremely difficult to quantify due to imaging limitations. However, despite this difficulty in measurement, focal adhesion clusters were shown to respond to structural stiffness by increasing in length in areas of higher stiffness as shown in Figure 15
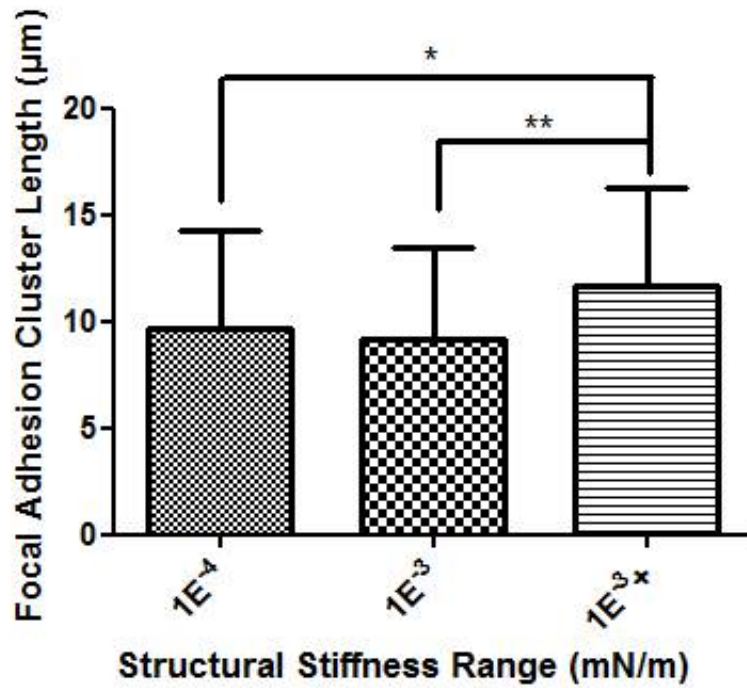
Figure 15. Focal adhesion cluster length is directly related to structural stiffness. Length of concentrated focal adhesion clusters increases with increased structural stiffness.

As seen in Figure 15, focal adhesion length is shown to increase at areas of high structural stiffness. Average focal adhesion length increases by over four μm from the lowest to highest stiffness area. This relationship holds for each fiber diameter tested, as shown in Figure 16.
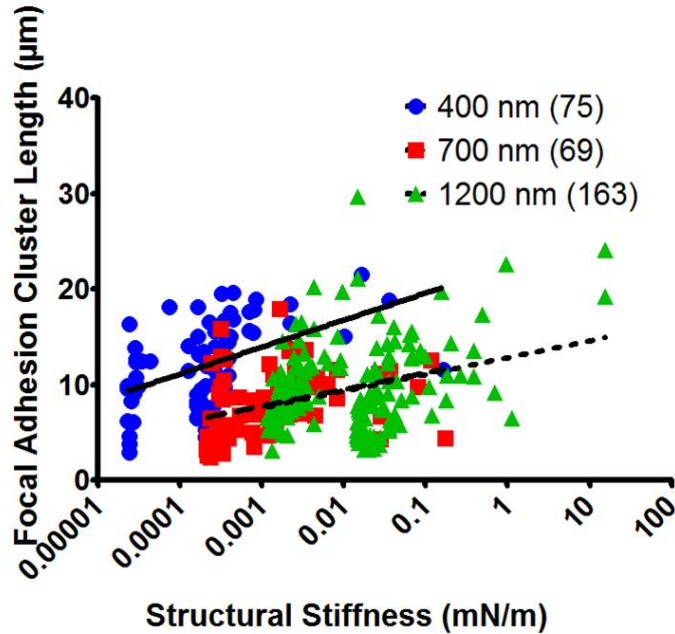
Figure 16. Focal adhesion length increases with increasing structural stiffness. This relationship holds for all fiber diameters

In Figure 16, it can be seen that there is a sizable difference between the length of focal adhesion clusters on 400 nm diameter fibers and larger diameter fibers at the same structural stiffness. This implies that the length of focal adhesion clusters is to some extent dependent on fiber curvature as well as structural stiffness. This relationship is explored further in section 4.7.

4.6.2 Nuclear Shape Index

Nuclear shape index has previously been shown to be an indicator of overall cell elongation and alignment [62]. Additionally, it has been shown that focal adhesions tend to increase in size on stiffer substrates, and cells subsequently increase their traction forces, leading to more stress on the cell body [25,63–65]. Therefore, nuclear shape index was the next cytoskeletal parameter explored. It was found that on single suspended nanofibers, nuclear

shape index decreases as cells reach areas of higher structural stiffness. This relationship can be

seen in Figure 17.
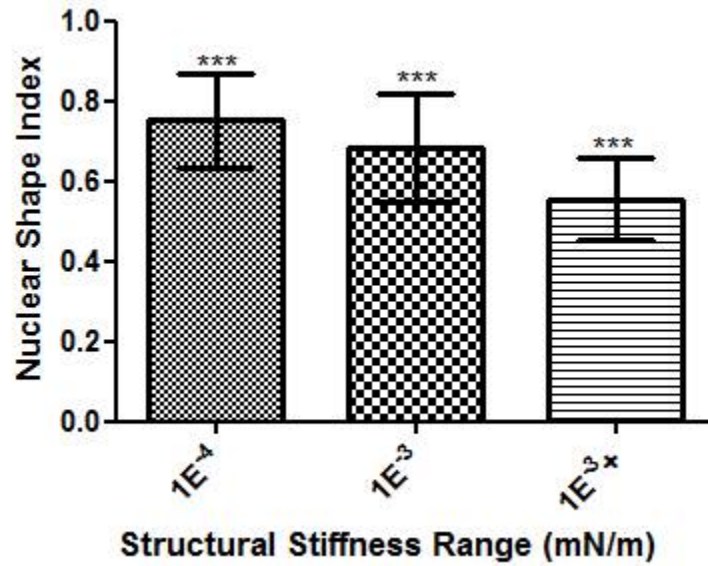
Figure 17. Nuclear shape index response to structural stiffness. As structural stiffness increases, nuclear shape index decreases. This is an indicator that cells are being subjected to higher stresses.

As seen Figure 17, nuclear shape index decreases with increasing structural stiffness,

which indicates that cells are being stretched so they elongate and flatten. This relationship can

be seen in Figure 18.
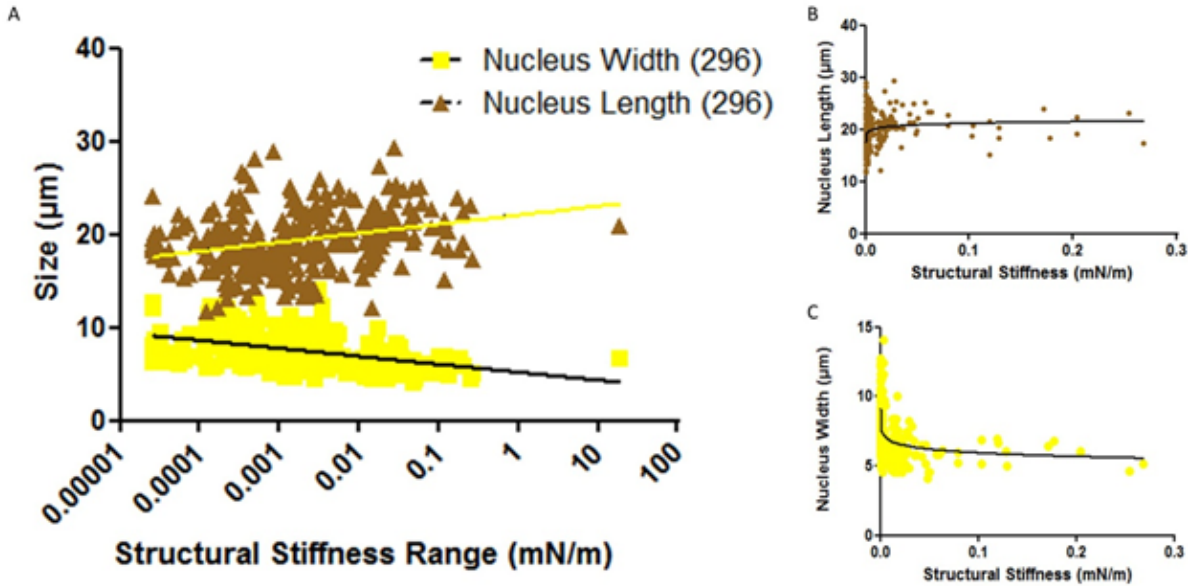
Figure 18.) Nucleus width and length response to structural stiffness. B) Nucleus length and
C) nucleus width both reach a threshold value and cannot increase/decrease any further.
The trends regarding the decrease in nuclear shape index were similar for all fiber

The trends regarding the decrease in nuclear shape index were similar for all fiber

diameters tested. The scatterplot that shows this data can be seen in Figure 19.
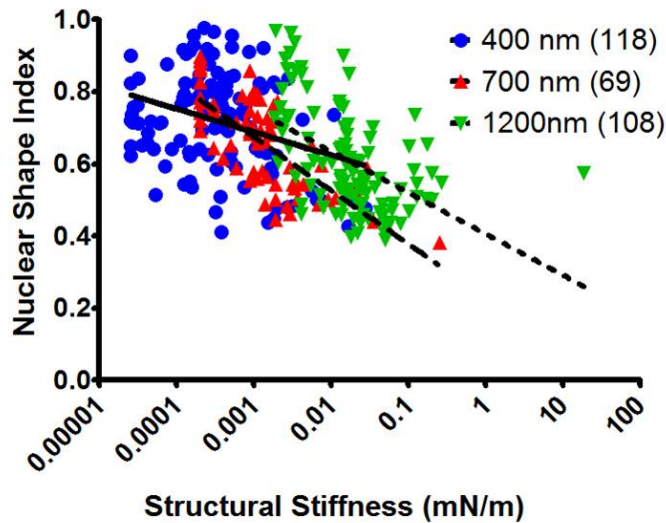
Figure 19. Nuclear shape index response to structural stiffness for each fiber diameter tested.
Although the slope of the trends change between fiber diameters, the trends all show
similar relationships between NSI and structural stiffness.

4.6.3 Overall Cell Length

The last cytoskeletal parameter that was explored was the overall cell length. This can be seen as an accompaniment to nuclear shape index in that as stress on the cell body increases due to substrate stiffness mechanosensing, the cell body is elongated by that stress. It is shown here that overall cell length increases with increasing structural stiffness, as seen in Figure 20.

This increase in length indicates that cells on the higher stiffness areas are putting more stress on the cell body, causing it to elongate. This result is corroborated by the increase in focal adhesion cluster length and the decrease in NSI that is shown in Figure 15 and Figure 17 respectively. Overall, these results signify that cells migrating along these single nanofibers are sensing and responding to changes in structural stiffness.
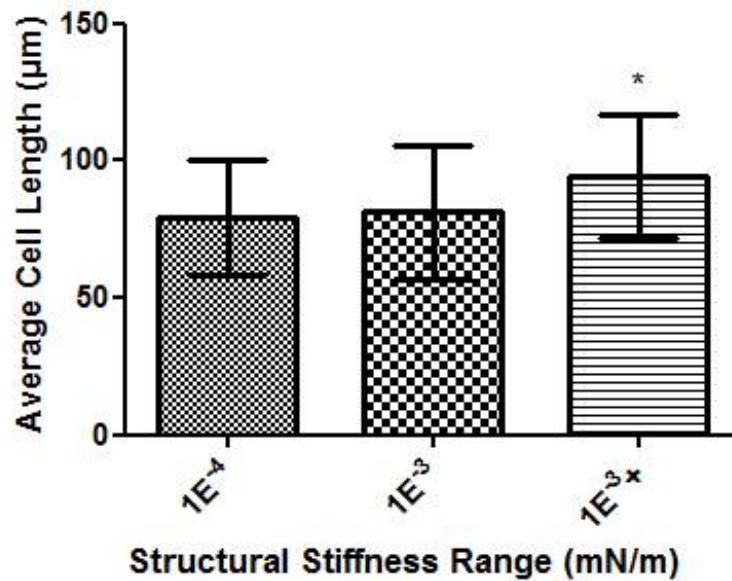
Figure 20. Overall cell body length increases as cells reach areas of higher structural stiffness.

The response of cell length to structural stiffness was also recorded for the separate fiber diameters tested. Figure 21 shows the results of these experiments.
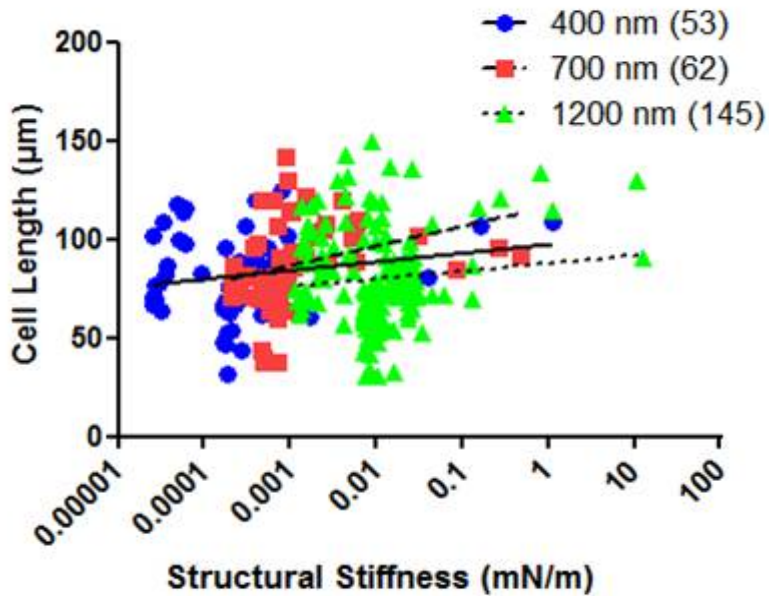
Figure 21. Cell length response to structural stiffness for each diameter tested. There is little fiber diameter dependence shown here.

4.7. Effects of Curvature on Cell Behavior

As seen in the previous sections fiber diameter has a direct influence on many of the considered cell behaviors. This is of interest because even at similar structural stiffness values some diverging effects are seen indicating that there could be even more to the cell/fiber substrate interaction than what has been characterized by looking at the structural stiffness. Additionally, previous studies have shown that substrate curvature can affect migration and cytoskeletal arrangement [66,67]. In this system, curvature can be investigated in a unique way, as the curvature presented to the cells is dependent on the diameter of the fiber. The effects of fiber diameter on each of the parameters studied are shown here. All effects were explored at a common structural stiffness value in the range on $1E^{-3}$ mN/m. This value was the point at which data was present for all fiber diameters most often.

4.7.1 Curvature Effects on Migration Speed

While migration speed decreased in response to an overall increase in fiber structural stiffness, fiber diameter has the opposite relationship with migration speed, where increasing fiber diameter at a single structural stiffness values causes increased migration speed to increase, as shown in Figure 22.
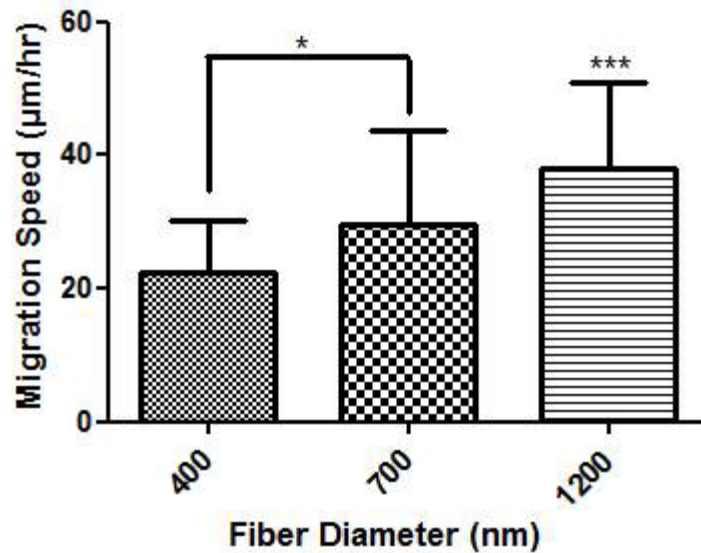
Figure 22. Effects of fiber diameter on migration speed at a single structural stiffness value (1E-3mN/m).

This relationship is notable because structural stiffness is partly dependent on the fiber diameter, and smaller diameter fibers tend to make up the lower structural stiffness areas where overall migration speed is highest, as seen in Figure 8. However, when the migration speed is compared at a common structural stiffness value between all three fiber diameters, cells move significantly faster on larger fibers. Because focal adhesion size and migration speed are closely

related, the focal adhesion length dependence on curvature was also explored to understand the effect of fiber diameter on migration speed.

4.7.2 Curvature Effects on Focal Adhesion Cluster Length

The primary mechanotransduction element in migrating cells has been shown to be the focal adhesions. Focal adhesion clusters were shown to increase in length with increasing structural stiffness in Figure 15. However, an opposite relationship between focal adhesion cluster length and fiber diameter is found when data points are compared at a similar structural stiffness value.
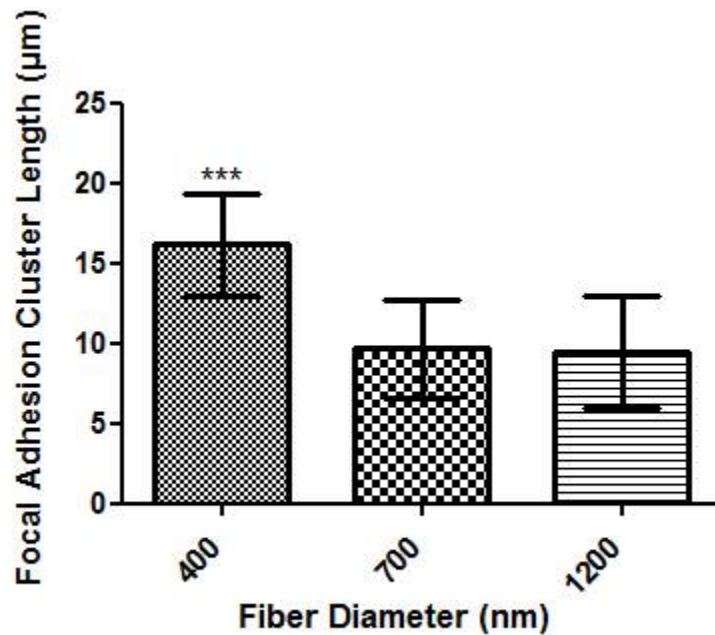
Figure 23. Effects of fiber diameter on focal adhesion cluster length at a single structural stiffness value (1E-3mN/m)

As shown above (Figure 23), focal adhesion cluster length decreases on fibers of larger diameter at a single structural stiffness value. This is again, the opposite trend that is seen when comparing focal adhesion cluster length and structural stiffness. This result along with the migration speed relationship seen in Figure 22 raises a few interesting questions regarding the structure of focal adhesions, how they interact with fibers, and the effects that this interaction has on both focal adhesion size and migration.

4.7.3 Focal Adhesion Area Conservation

When studying focal adhesions on two dimensional substrates, focal adhesion area is typically the measured parameter. There have been many studies that have linked this area to migration behavior and cytoskeletal arrangement[25,68,69]. The general observed trend is an increase in focal adhesion area corresponds to increases in cell traction forces, which in turn leads to a decrease in migration speed. This causes higher stresses on the cell body, leading to a flatter nucleus and highly stretched cell body [3,70,71]. This measurement metric is difficult to compare to cells on fibers, as for a cell-fiber system the focal adhesions are concentrated at the poles of the cells, and cluster together to form a large focal adhesion patch instead of several smaller focal adhesions along the periphery of the cell. There is also the problem of not being able to see the degree to which these focal adhesions patches curve around the fiber.
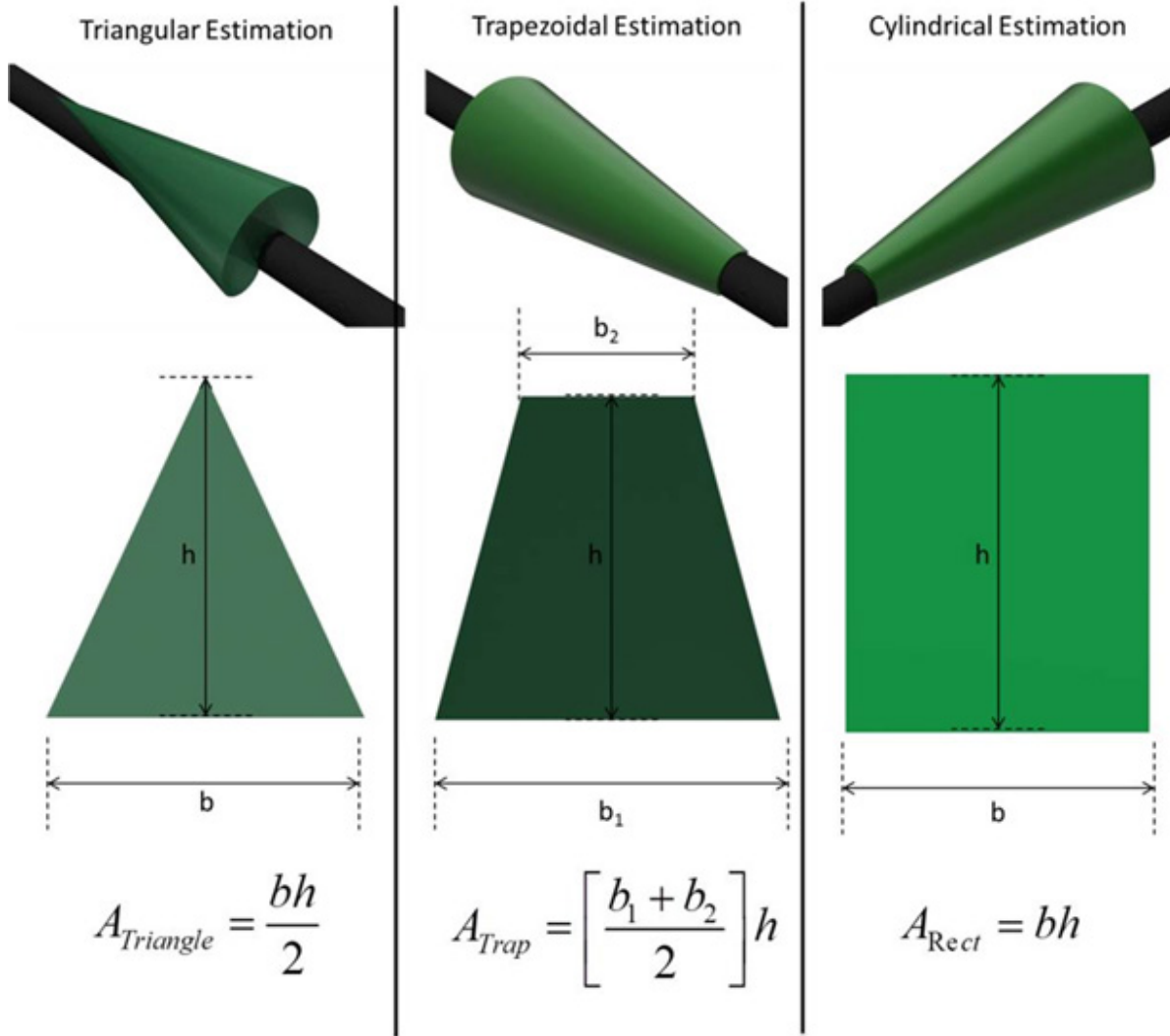
Figure 24. Three different possible focal adhesion patch configurations used to estimate focal adhesion area.

Ongoing efforts to quantify this wrapping with confocal images and electron microscopy, are still in their infancy. However, by applying simple Hertzian mechanics simulating the problem of a soft body cell wrapping around a relatively stiffer fiber, the degree of wrapping and therefore focal adhesion area can be estimated. The procedure used to estimate this wrapping can be seen in Appendix B.1. This was done in three ways that explored three different possible focal adhesion patch configurations, a triangular, cylindrical, and trapezoidal shape. These arrangements along with the equations that dictate their area can be seen below in Figure 24.

Using the arrangements shown above, the focal adhesion area for each diameter at three common structural stiffness values was compared. This comparison, along with the focal adhesion cluster length at the same intervals is shown in Figure 25.
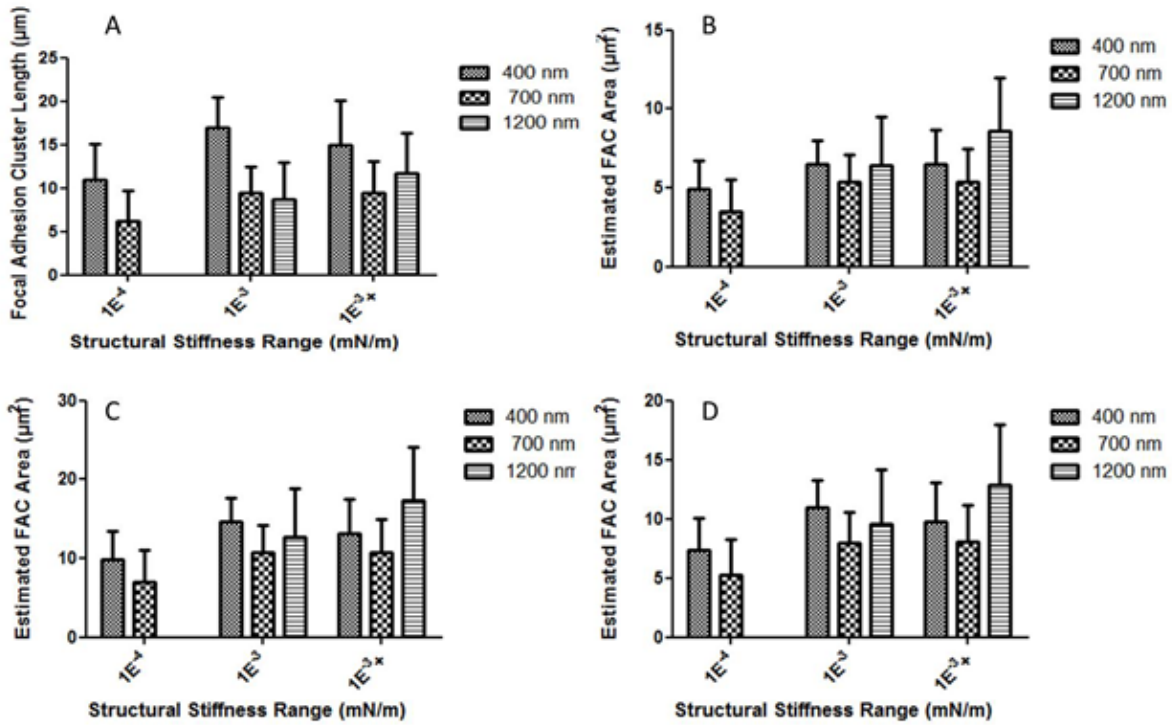
Figure 25. Focal adhesion length (A), and area using the triangular configuration (B), cylindrical configuration (C), and trapezoidal configuration (D).

As seen in Figure 25, focal adhesion cluster length increases dramatically on the smallest diameter fibers. This is the first indication that the area may be conserved between diameters at similar stiffness values. This relationship can be seen in the rest of Figure 25 for each of the configurations shown in Figure 24. In each configuration, the focal adhesion area is very small at low stiffness values and increases with increasing stiffness, which matches studies showing focal adhesion area increases on substrates with higher Young's modulus [65,70,72]. More

interestingly, the disparity seen in focal adhesion cluster length between 400 nm diameter and the larger diameter fibers almost disappears when focal adhesion cluster area is considered instead of length. This result indicates that the sensing mechanism that dictates focal adhesion arrangement is exclusively responding to structural stiffness and modulating the area in response to stiffness while also compensating for the different fiber diameters. This could be interpreted in two ways: Either cells are disregarding the curvature effect and just modulating focal adhesion area based on structural stiffness, or cell are taking into account both of these parameters and modulating focal adhesion area in response to both. Either of these interpretations raises interesting questions about cellular mechanosensing and the parameters that cells take into account when modulating their cytoskeletal arrangement. Investigating the relationship between focal adhesion area and structural stiffness could lead to important insights into the process of mechanosensing, but being able to accurately observe this area on fibers is an obstacle that needs to be overcome.

4.7.4 Curvature Effects on NSI and Cell Length

The effects of fiber diameter were overall less pronounced on the nuclear shape index and overall cell length. Comparisons of these parameters for each fiber diameter at a single structural stiffness value ($1E^{-3}$ mN/m) are shown in Figure 26 and Figure 27 respectively. For these parameters, there was no significant trend in their relationship with fiber diameter. This further supports the conclusion that was drawn from the relationship between focal adhesion area and structural stiffness. These results support the suggestion that cells are responding only to the structural stiffness value of the fiber they are traveling, and getting limited input from the physical confinement due to being cultured on a single nanofiber.

44
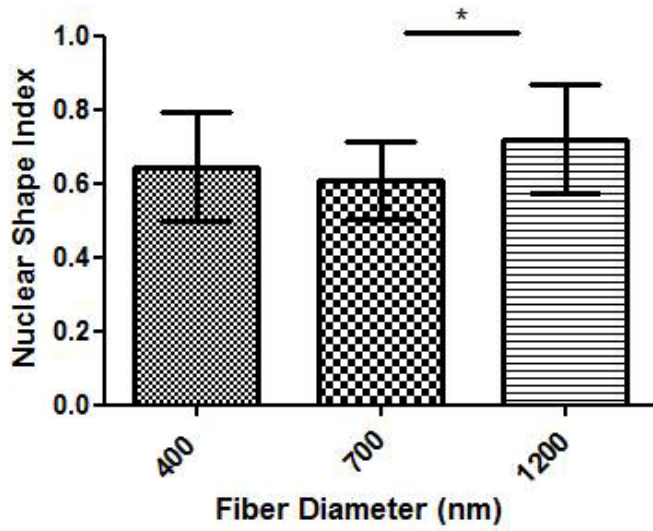
Figure 26. Effects of fiber diameter on NSI at a single structural stiffness value (1E-3 mN/m)
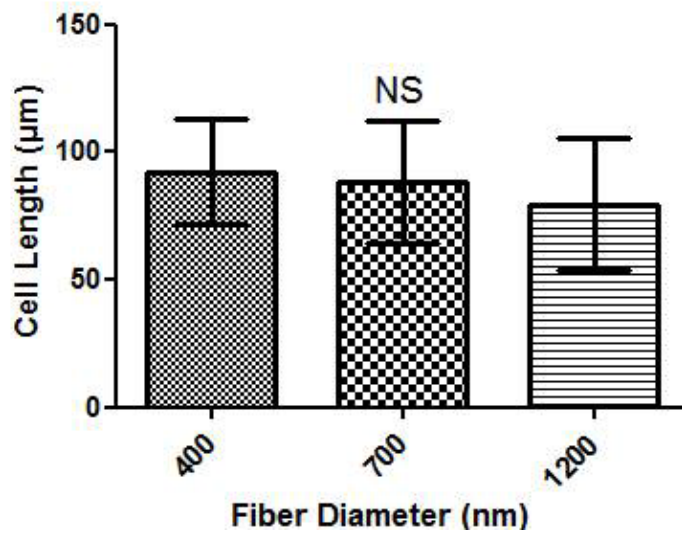
Figure 27. Effects of fiber diameter on cell length at a single structural stiffness value (1E-3 mN/m)

4.8. Rate of Cell Spreading and Migration Commencement

A brief analysis of the time taken for cells to both reach their fully spread state as well as the time taken to begin migration after seeding was conducted. While the results shown here are

not statistically significant, the trends that are defined raise some interesting questions as further support the hypothesis that cells are responding to changes in structural stiffness is a myriad of way. As seen in Figure 28, cells both reach their fully spread state and begin migrating faster on areas of higher structural stiffness. This could be an indicator of faster actin filament formation or focal adhesion turnover. The effect of structural stiffness on the rate of these activities warrants further exploration.
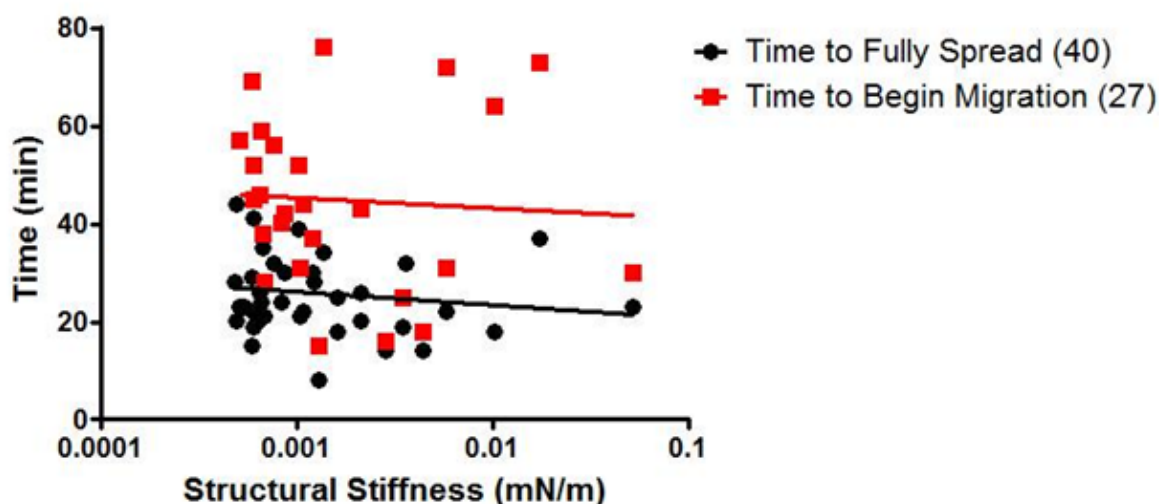
Figure 28. The amount of time that cells took after seeding to reach their fully spread state and then begin migration decreased with increasing structural stiffness.

Chapter Five: Discussion

5.1. Scaffold Design and Parameter Control

Scaffolds for characterization of cellular migration and cytoskeletal arrangement were created in a repeatable fashion using an integration of hand fabrication, soft lithography, and the STEP nanofiber deposition technique. The creation of several scaffold types, all suitable for different testing circumstances, was explored. Ultimately, hand fabrication of substrates with

PDMS blocks acting as raised constructs for fiber boundary control were the most suitable for the specific experiments here, but the process to create micropillar based substrates was fully realized, which could be utilized to create substrates suitable for experiments involving traction forces and fiber stiffness modulation.

Fiber length and diameter was controlled using the STEP method, which has been previously shown to allow for control over these parameters. The level of control afforded by this method of fiber deposition allowed for the creation of substrates with repeatable structural stiffness gradients, and changing the fiber diameter and length allowed for exploration of a wide range of structural stiffness values. Additionally, control over the fiber spacing ensured that cells were only able to interact with a single fiber.

Structural stiffness at several points along a single fiber was measured via AFM, and was found to be very low at the middle of the span length of each fiber, and increase sharply near the ends. This relationship was shown to hold for all fiber diameters and lengths, and to match the equivalent spring constant model reasonably well. However, continued improvement to both the theoretical model as well as the AFM measurement techniques could provide additional insights into the relationship between cellular behavior and structural stiffness.

5.2. Substrate Dimensionality

One of the important factors that has been shown to affect single cell migration and cytoskeletal arrangement is the dimensionality of the substrates they are interacting with. Currently, substrate dimensionality is divided into three main categories: two dimensional, three dimensional, and one dimensional.

Two dimensional substrates consist of a cell interacting with a flat, unconfined space. The majority of i*n vitro* experimentation has been performed using substrates of this type. The most common substrates used are either glass cover slides or polymer gels (collagen, PDMS, etc.) However the accuracy of cell-substrate interaction in two dimensional experiments to actual *in vivo* conditions has come into question [6]. Therefore, many studies have moved to using three dimensional substrates to study cell behavior. These substrates normally consist of a gel with controllable physical properties like pore size, density, and degree of crosslinking. Cells travel through these constructs, interacting with the three dimensional architecture. Three dimensional constructs are thought to provide the closest approximation to *in vivo* conditions that is possible, but with this comes increased difficulty in controlling the parameters that affect cellular migration. One dimensional substrates involve restricting cellular migration to a single line using ligand patterning. While these are most likely the substrate type that is furthest from *in vivo* conditions, studies have shown that many characteristics of cellular migration on one dimensional substrates more closely match three dimensional conditions than two dimensional [36]. Each of these substrate types show different cellular responses to substrate stiffness and other physical parameters, which has led to a large amount of knowledge regarding cell-substrate interactions. However, the specific dimensionality of using single nanofibers as cell migration scaffolds is a complicated intricacy.

5.2.1 Single Nanofiber Dimensionality

The dimensionality of the system presented in this work is an interesting question without a simple answer. Because cells are limited to traveling along a single nanofiber, they can only migrate in a single direction and its reverse along a single line. This restriction creates a clear

similarity to one dimensional systems. However, the cross section of the fibers that cells are traveling along are round, and cells wrap around the fibers. While the extend of this wrapping has not been able to be confirmed at this point, simple Hertzian contact mechanic simulations show that cells will wrap mostly around the fibers at each of these low diameters. This is further corroborated by the fact that normal cell spread area is much larger than the fiber diameter. Due to this wrapping, characterizing the dimensionality of cells traveling along these nanofibers is difficult.

5.3. Cellular Response to Structural Stiffness

The response of single cells to the gradient of structural stiffness along a single fiber in both their migration characteristics and cytoskeletal arrangement has been explored in this study. Overall, these responses have implied that there is an active stiffness sensing mechanism that allows cells to probe the physical properties of single nanoscale fibers and modulate their behavior in response to both structural stiffness in a way that is comparable to cellular response to substrates with changing Young's modulus. However, these responses occur with no change in material properties, relying only on the nanofiber arrangement to provide a gradient of structural stiffness.

5.3.1 Migration Response to Structural Stiffness

Sections 4.3 and 4.4 explore the relationships between single cell migration to changes in structural stiffness. The parameters that are of particular interest are migration speed and directionality. It was shown that cell migration speed decreases as cells reach areas of higher structural stiffness, and in Figure 11 it is shown that a majority of cellular migration takes place in the direction of higher stiffness (towards the fiber ends). These results together imply that

cells are actively searching for higher stiffness areas, and modulating their migration speed in order to reach those areas and then remain there. This behavior indicates that cells must be actively and constantly sensing the structural stiffness of their substrate through substrate interaction and changing their behavior in response to what they sense. This could lead to important insights into how cells choose to migrate both in the body and during *in vitro* experimentation. The behaviors shown here suggest that cells are responding to the physical environment in their immediate area, and sensing substrate stiffness at a previously unexplored level.

The cellular response to structural stiffness in comparison to previously published studies that look at changing substrate Young's modulus bears some interesting resemblances. At a very base level, there are a few cellular responses to changing substrate Young's modulus that tend to hold for many cell types and substrate configurations. Lo et al. and Raab et al. have both shown that cell will tend to migrate in the direction of increased Young's modulus on flat substrate [48,59]. Additionally, it has been shown that migrating cells will both decrease their migration speed in relation to increased substrate modulus [70], and will tend to migrate onto areas of higher substrate modulus and remain there [73,74]. These results all indicate that cells are sensing changes in the modulus of their substrate and responding by preferentially moving towards those areas of higher modulus and remaining there.

These results are basically directly parallel to what has been observed here in cells migrating along single nanofibers. However, when a cell is migrating along a nanofiber and interacting with nothing else, there is no change in modulus along the length of that fiber. What does change along that length is the structural stiffness of the fiber, indicating that cells also

50

sense and respond to this parameter when adapting their migration to their physical environment. This in turn raises questions about the comparative effects of substrate modulus and structural stiffness.

5.3.2 Cytoskeletal Response to Structural Stiffness

As mentioned earlier, focal adhesions are primarily responsible for communicating both physical and chemical information from the substrate a cell is interacting with to the cell. Cells take both physical and chemical cues from their substrate and alter their behavior based on these cues. Therefore, the response of focal adhesions and other cytoskeletal components can be important indicators to occurrences in cell substrate interaction. Some of the most exhaustively studied cytoskeletal parameters include cell area, focal adhesion configuration, and nuclear shape. In this study these parameters are explored in Figure 21, Figure 15, and Figure 17 respectively.

Like shown in Section 5.3.1, the response of most of these cytoskeletal components to structural stiffness is noticeably similar to their response to changing substrate modulus, with some minor caveats due to the physical restrictions placed on cell geometry due to the fiber substrate. On two dimensional substrates, cells have been shown to respond to increasing substrate modulus by: increasing focal adhesion length and area [28], increasing their spread area [68,75], and increasing the stress on the nucleus, causing it to flatten [56]. The cellular response to increasing structural stiffness is that cells will increase their focal adhesion cluster length, increase their overall cell length, and decrease the nuclear shape index. When the geometrical constraints placed on the cells that are attached to a single fiber are taken into account, the focal adhesion cluster length and cell length can be seen as analogous to the two

51

dimensional substrate parameters of focal adhesion area and cell area. Therefore, the cellular behavior in response to these stiffness parameters are similar.

5.4. Focal Adhesion Area Reliance on Structural Stiffness

Previous studies have shown that focal adhesion size and cellular motility are highly linked, where chemically reducing focal adhesion size leads to increased migration and decreased persistence, and using changing modulus to influence migration and cytoskeletal arrangement which leads to increased focal adhesion area [76,77]. This study has shown similar results, where higher structural stiffness leads to increased focal adhesion length as well as increased estimated focal adhesion area, as seen in Figure 15 and Figure 25 respectively. The same structural stiffness areas that exhibit increased focal adhesion appearance also exhibit decreased migration speed, as seen in Figure 9. Therefore, it can be extrapolated that increased focal adhesion size correlates to decreased migration speed.

As seen in Figure 25, focal adhesions cluster length is significantly increased on small diameter fibers in comparison to the larger diameter fibers at similar structural stiffness values. However, if the focal adhesion area is estimated and plotted at the same diameters and stiffness values, the difference between focal adhesion area on each fiber diameter becomes much smaller. This indicates that the sensing mechanism that dictates focal adhesion configuration is responding primarily to structural stiffness and attempting to respond to changing structural stiffness by adjusting focal adhesion area the same way regardless of fiber diameter.

These results, along with the lack of significant response in cell length and NSI to changing diameter, indicate that while confining cells to single suspended nanofibers does considerably

affect the cytoskeletal arrangement when compared to cells cultured on flat substrates, cells respond almost exclusively to structural stiffness, and perhaps masking fiber diameter effects. This implication could have some interesting effects on the view of the interplay between stiffness and substrate dimensionality. However, when comparing the characteristic scale of the elongated cell length ($\approx$100µm) and width ($\approx$10's µm) with the fiber diameter ($\approx$100's nm), there is a large disparity in between these scales. Further investigation into the relationship between structural stiffness and fiber diameter would benefit from investigation of higher fiber diameters that are closer to a characteristic cell size.

Chapter Six: Conclusions

Previous research has shown that the physical properties of a cell's substrate has profound effects on many cellular behaviors, including motility and cytoskeletal arrangement. One of the most extensively studied physical parameters is the substrate Young's modulus. This has led to important advances in the understanding of cell substrate interactions as a whole. This study has shown that similar changes in cellular behavior can be seen in cells responding to the structural stiffness of a single nanofiber with no changes in Young's modulus.

This study presents a method of exploring cellular mechanosensing utilizing a single suspended PS nanofiber to provide a physically constrained mechanical environment that presents a gradient of structural stiffness. Structural stiffness is shown to be lowest at the center of the fiber and increase sharply near the fixed fiber ends. Additionally, three fiber diameters (400, 700, and 1200 nm) and two fiber lengths (1 and 2 mm) are used to present a large range of structural stiffness values to migrating cells. Fibers were deposited over PDMS blocks using the STEP method, which allowed for a high degree of alignment and spacing to ensure cells did not interact with more than one fiber simultaneously.

Using the custom single cell-fiber system, cells were observed to respond to increasing structural stiffness is several quantifiable ways. The first observed response was cells decreasing their migration speed, and also preferentially migrating in the direction of increasing stiffness. Because cellular migration and mechanosensing are both highly dependent upon cytoskeletal arrangement, cells were immunostained for focal adhesions, F-actin stress fibers, and nuclei. From these studies it was found that cell length and focal adhesion cluster length both increased

with increasing structural stiffness, and NSI decreased with increasing structural stiffness as nuclei became elongated. Additionally, estimation of the focal adhesion area indicated that while overall area increases with structural stiffness, it is similar between all fiber diameters at comparable structural stiffness values. This result along with recent studies that have shown the importance of focal adhesion size to migration characteristics suggest that cells are modulating their focal adhesion maturity and size in response to structural stiffness, which leads to both decreased migration and could lead to increased traction forces as well as increased stress placed on the cell body, causing an increases in cell length and nucleus.

These results all indicate that cells are sensing and responding to structural stiffness by modulating their cytoskeletal arrangement, applied traction, and migration speed. These responses are similar to what has been shown on flat gel substrates with varying Young's modulus however, on nanofibers there is no change in modulus. These results are a strong indicator that cells perform mechanosensing beyond the traditionally accepted bulk modulus sensing, and may be responding to structural stiffness in gel and fibrous constructs that are currently used in many research scenarios. The effects of structural stiffness need to be considered in future studies, and further exploration of this relationship could lead to important insights into cellular mechanosensing.

6.1. Future Work

Future work regarding the relationship between structural stiffness and cellular behavior has many avenues that warrant exploration. Further exploration of the focal adhesion dynamics in real time using transfected cells could improve understanding of how cells are sensing structural stiffness and modulating their cytoskeleton in response. Additionally, the

implementation of an in house fiber stretching apparatus integrated into the AxioVision Z.1 microscope would allow for modulation of fiber tension and structural stiffness in real time. Preliminary designs of this setup can be seen in Figure 29.
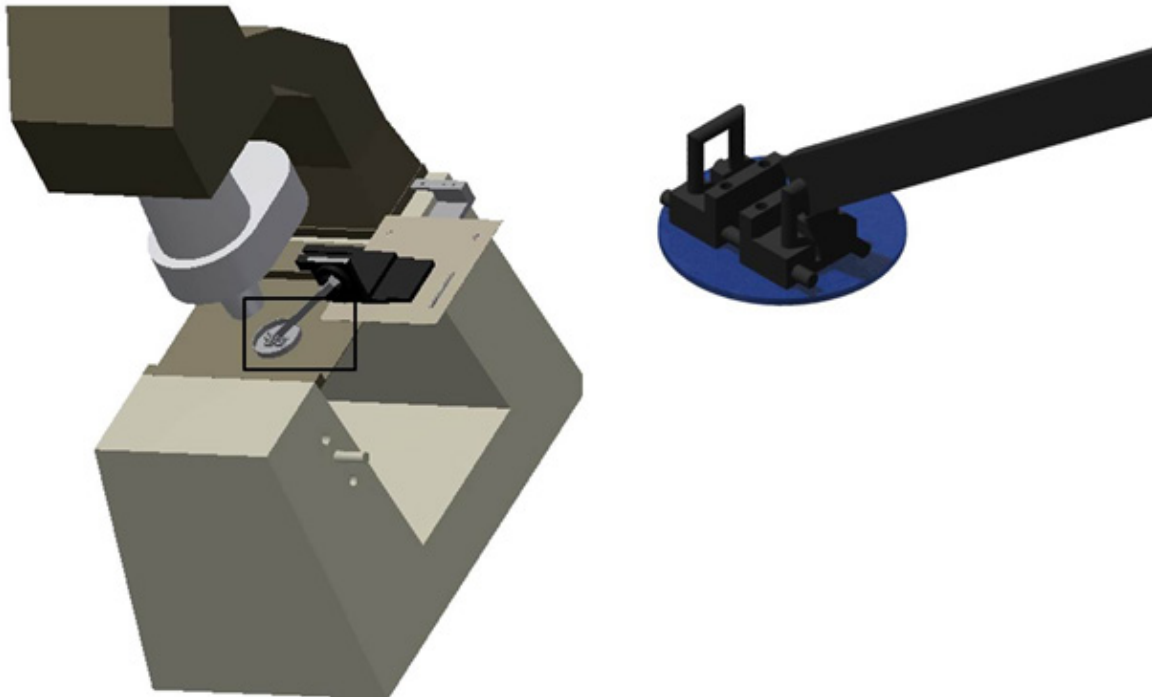
Figure 29. Preliminary design of fiber stretching apparatus. Integration into a microscope would allow for real time imaging of cells presented with changing structural stiffness, which could further enhance understanding of this relationship.

The design seen in Figure 29 allows for manipulation of substrates like the ones used in this study, and is designed to be integrated into the AxioVision Z.1 microscope. It will use a Sutter MP 285 Micromanipulator to stretch aligned fibers during time lapse imaging. This would allow for studies in which the fiber structural stiffness was modified by changing the fiber tension. These could be performed to augment understanding of the mechanosensing mechanism that allows for cellular response to structural stiffness as well as for simulation of mechanical

stress on cells, which has been shown to be an important physical property in differentiation and cellular behavior.

In addition to exploring the response of cells to dynamic structural stiffness values, there are several uncharacterized cellular behaviors that warrant further exploration of the cellular response to the innate gradient of structural stiffness present in nanofibers. Of particular interest are parameters like probability of mitosis and rate of actin polymerization. A cursory exploration of the rate of cell spreading in response to structural stiffness has been performed, which has shown that there is some tendency for cells to reach their fully spread state faster on areas of higher structural stiffness, as seen in Figure 28. This could be an indicator of a faster rate of actin stress fiber or focal adhesion formation. Studies of this type could provide further information regarding the nuances of cellular response to structural stiffness.

The focus of future work should lie in understanding the specific cellular mechanics that allow for mechanosensing of structural stiffness and their implementation in both experimental design and product planning. The effect of substrate modulus has been an area of intense study recently, and the findings in this area have begun to be considered in many studies that would have previously been performed on two dimensional glass substrates. The same principles regarding structural stiffness needs to be taken into account, especially as many of those studies are moving from glass substrates to fibrous constructs or gels with complex fibrous microarchitecture.

Chapter Seven: Referenced Works

[1]   Pizzo a M., Kokini K., Vaughn L. C., Waisner B. Z., and Voytik-Harbin S. L., 2005, "Extracellular matrix (ECM) microstructural composition regulates local cell-ECM biomechanics and fundamental fibroblast behavior: a multidimensional perspective.," Journal of applied physiology (Bethesda, Md. : 1985), **98**(5), pp. 1909–21.

[2]   Gardel M., and Schwarz U., 2010, "Cell-substrate interactions.," Journal of physics. Condensed matter : an Institute of Physics journal, **22**(19), p. 190301.

[3]   Pedersen J. a, and Swartz M. a, 2005, "Mechanobiology in the third dimension.," Annals of biomedical engineering, **33**(11), pp. 1469–90.

[4]   Frantz C., Stewart K. M., and Weaver V. M., 2010, "The extracellular matrix at a glance.," Journal of cell science, **123**(Pt 24), pp. 4195–200.

[5]   Reilly G. C., and Engler A. J., 2010, "Intrinsic extracellular matrix properties regulate stem cell differentiation.," Journal of biomechanics, **43**(1), pp. 55–62.

[6]   Pathak A., and Kumar S., 2011, "Biophysical regulation of tumor cell invasion: moving beyond matrix stiffness.," Integrative biology : quantitative biosciences from nano to macro, **3**(4), pp. 267–78.

[7]   Anderson R. K., Anderson E., Shakir L., and Glover S. C., 2006, "Image Analysis of Extracellular Matrix Topography of Colon Cancer Cells," (C), pp. 5–7.

[8]   Cox T. R., and Erler J. T., 2011, "Remodeling and homeostasis of the extracellular matrix: implications for fibrotic diseases and cancer.," Disease models & mechanisms, **4**(2), pp. 165–78.

[9]   Lu P., Weaver V. M., and Werb Z., 2012, "The extracellular matrix: a dynamic niche in cancer progression.," The Journal of cell biology, **196**(4), pp. 395–406.

[10]   Pathak A., and Kumar S., 2011, "Biophysical regulation of tumor cell invasion: moving beyond matrix stiffness.," Integrative biology : quantitative biosciences from nano to macro, **3**(4), pp. 267–78.

[11]   Pathak A., and Kumar S., 2012, "Independent regulation of tumor cell migration by matrix stiffness and confinement.," Proceedings of the National Academy of Sciences of the United States of America, **109**(26), pp. 10334–9.

[12]   Bao G., and Suresh S., 2003, "Cell and molecular mechanics of biological materials.," Nature materials, **2**(11), pp. 715–25.

[13]   Beningo K. a, Lo C.-M., and Wang Y.-L., 2002, "Flexible polyacrylamide substrata for the analysis of mechanical interactions at cell-substratum adhesions.," Methods in cell biology, **69**, pp. 325–39.

[14]   Dieterich P., Klages R., Preuss R., and Schwab A., 2008, "Anomalous dynamics of cell migration.," Proceedings of the National Academy of Sciences of the United States of America, **105**(2), pp. 459–63.

[15]   Harley B. a C., Kim H.-D., Zaman M. H., Yannas I. V, Lauffenburger D. a, and Gibson L. J., 2008, "Microarchitecture of three-dimensional scaffolds influences cell migration behavior via junction interactions.," Biophysical journal, **95**(8), pp. 4013–24.

[16]   Guo W., Frey M. T., Burnham N. a, and Wang Y., 2006, "Substrate rigidity regulates the formation and maintenance of tissues.," Biophysical journal, **90**(6), pp. 2213–20.

[17]   Lauffenburger D. a, and Horwitz a F., 1996, "Cell migration: a physically integrated molecular process.," Cell, **84**(3), pp. 359–69.

[18]   Friedl P., and Wolf K., 2009, "Proteolytic interstitial cell migration: a five-step process.," Cancer metastasis reviews, **28**(1-2), pp. 129–35.

[19]   Kandere-Grzybowska K., Soh S., Mahmud G., Komarova Y., Pilans D., and Grzybowski B. a., 2010, "Short-term molecular polarization of cells on symmetric and asymmetric micropatterns," Soft Matter, **6**(14), p. 3257.

[20]   Seetapun D., and Odde D. J., 2010, "Cell-Length-Dependent Microtubule Accumulation during Polarization," Current Biology, **20**(11), pp. 979–988.

[21]   Huttenlocher A., 2005, "Cell polarization mechanisms during directed cell migration.," Nature cell biology, **7**(4), pp. 336–7.

[22]   Xue F., Janzen D. M., and Knecht D. a, 2010, "Contribution of Filopodia to Cell Migration: A Mechanical Link between Protrusion and Contraction.," International journal of cell biology, **2010**, p. 507821.

[23]   Brunette D. M., 1986, "Spreading and orientation of epithelial cells on grooved substrata.," Experimental cell research, **167**(1), pp. 203–17.

[24]   Dalby M. J., 2007, "Cellular response to low adhesion nanotopographies," International Journal, **2**(3), pp. 373–381.

[25]   Rape A. D., Guo W.-H., and Wang Y.-L., 2011, "The regulation of traction force in relation to cell shape and focal adhesions.," Biomaterials, **32**(8), pp. 2043–51.

[26] Zebda N., Dubrovskyi O., and Birukov K. G., 2011, "Focal Adhesion Kinase Regulation of Mechanotransduction and its Impact on Endothelial Cell Functions.," Microvascular research, **83**(1), pp. 71–81.

[27] Schwarz U. S., Balaban N. Q., Riveline D., Bershadsky a, Geiger B., and Safran S. a, 2002, "Calculation of forces at focal adhesions from elastic substrate data: the effect of localized force and the need for regularization.," Biophysical journal, **83**(3), pp. 1380–94.

[28] Kim D.-H., and Wirtz D., 2012, "Focal adhesion size uniquely predicts cell migration.," FASEB journal : official publication of the Federation of American Societies for Experimental Biology, pp. 1351–1361.

[29] Gardel M., and Schwarz U., 2010, "Cell-substrate interactions.," Journal of physics. Condensed matter : an Institute of Physics journal, **22**(19), p. 190301.

[30] Fournier M. F., Sauser R., Ambrosi D., Meister J.-J., and Verkhovsky A. B., 2010, "Force transmission in migrating cells.," The Journal of cell biology, **188**(2), pp. 287–97.

[31] Harley B. a C., Kim H.-D., Zaman M. H., Yannas I. V, Lauffenburger D. a, and Gibson L. J., 2008, "Microarchitecture of three-dimensional scaffolds influences cell migration behavior via junction interactions.," Biophysical journal, **95**(8), pp. 4013–24.

[32] Pek Y. S., Wan A. C. a, and Ying J. Y., 2010, "The effect of matrix stiffness on mesenchymal stem cell differentiation in a 3D thixotropic gel.," Biomaterials, **31**(3), pp. 385–91.

[33] Oakes P. W., Patel D. C., Morin N. a, Zitterbart D. P., Fabry B., Reichner J. S., and Tang J. X., 2009, "Neutrophil morphology and migration are affected by substrate elasticity.," Blood, **114**(7), pp. 1387–95.

[34] Raab M., Swift J., P. Dingal P. C. D., Shah P., Shin J.-W., and Discher D. E., 2012, "Crawling from soft to stiff matrix polarizes the cytoskeleton and phosphoregulates myosin-II heavy chain," The Journal of Cell Biology, **199**(4), pp. 669–683.

[35] Liu Y., Franco A., Huang L., Gersappe D., Clark R. a F., and Rafailovich M. H., 2009, "Control of cell migration in two and three dimensions using substrate morphology.," Experimental cell research, **315**(15), pp. 2544–57.

[36] Doyle A. D., Wang F. W., Matsumoto K., and Yamada K. M., 2009, "One-dimensional topography underlies three-dimensional fibrillar cell migration.," The Journal of cell biology, **184**(4), pp. 481–90.

[37] Legant W. R., Miller J. S., Blakely B. L., Cohen D. M., Genin G. M., and Chen C. S., 2010, "Measurement of mechanical tractions exerted by cells in three-dimensional matrices.," Nature methods, **7**(12), pp. 969–71.

[38]   Fischer R. S., Myers K. a, Gardel M. L., and Waterman C. M., 2012, "Stiffness-controlled three-dimensional extracellular matrices for high-resolution imaging of cell behavior.," Nature protocols, **7**(11), pp. 2056–66.

[39]   Carey S. P., Kraning-Rush C. M., Williams R. M., and Reinhart-King C. a, 2012, "Biophysical control of invasive tumor cell behavior by extracellular matrix microarchitecture.," Biomaterials, **33**(16), pp. 4157–65.

[40]   Janmey P. a, and Miller R. T., 2011, "Mechanisms of mechanical signaling in development and disease.," Journal of cell science, **124**(Pt 1), pp. 9–18.

[41]   Engler A. J., Sen S., Sweeney H. L., and Discher D. E., 2006, "Matrix elasticity directs stem cell lineage specification.," Cell, **126**(4), pp. 677–89.

[42]   Engler A. J., Sen S., Sweeney H. L., and Discher D. E., 2006, "Matrix elasticity directs stem cell lineage specification.," Cell, **126**(4), pp. 677–89.

[43]   Moreo P., García-Aznar J. M., and Doblaré M., 2008, "Modeling mechanosensing and its effect on the migration and proliferation of adherent cells.," Acta biomaterialia, **4**(3), pp. 613–21.

[44]   Borau C., Kamm R. D., and García-Aznar J. M., 2011, "Mechano-sensing and cell migration: a 3D model approach.," Physical biology, **8**(6), p. 066008.

[45]   Kuo C.-H. R., Xian J., Brenton J. D., Franze K., and Sivaniah E., 2012, "Complex Stiffness Gradient Substrates for Studying Mechanotactic Cell Migration.," Advanced materials (Deerfield Beach, Fla.), pp. 6059–6064.

[46]   Reilly G. C., and Engler A. J., 2010, "Intrinsic extracellular matrix properties regulate stem cell differentiation.," Journal of biomechanics, **43**(1), pp. 55–62.

[47]   Parekh S. H., Chatterjee K., Lin-Gibson S., Moore N. M., Cicerone M. T., Young M. F., and Simon C. G., 2011, "Modulus-driven differentiation of marrow stromal cells in 3D scaffolds that is independent of myosin-based cytoskeletal tension.," Biomaterials, **32**(9), pp. 2256–64.

[48]   Lo C. M., Wang H. B., Dembo M., and Wang Y. L., 2000, "Cell movement is guided by the rigidity of the substrate.," Biophysical journal, **79**(1), pp. 144–52.

[49]   Nain A. S., Sitti M., Jacobson A., Kowalewski T., and Amon C., 2009, "Dry Spinning Based Spinneret Based Tunable Engineered Parameters (STEP) Technique for Controlled and Aligned Deposition of Polymeric Nanofibers.," Macromolecular rapid communications, **30**(16), pp. 1406–12.

[50] Nain A. S., Phillippi J. a, Sitti M., Mackrell J., Campbell P. G., and Amon C., 2008, "Control of cell behavior by aligned micro/nanofibrous biomaterial scaffolds fabricated by spinneret-based tunable engineered parameters (STEP) technique.," Small (Weinheim an der Bergstrasse, Germany), **4**(8), pp. 1153–9.

[51] Kim M.-S., Choi J.-H., Kim J.-H., and Park Y.-K., 2010, "Accurate determination of spring constant of atomic force microscope cantilevers and comparison with other methods," Measurement, **43**(4), pp. 520–526.

[52] Peeters E. a G., Oomens C. W. J., Bouten C. V. C., Bader D. L., and Baaijens F. P. T., 2005, "Mechanical and failure properties of single attached cells under compression.," Journal of biomechanics, **38**(8), pp. 1685–93.

[53] Riboldi S. a, Sampaolesi M., Neuenschwander P., Cossu G., and Mantero S., 2005, "Electrospun degradable polyesterurethane membranes: potential scaffolds for skeletal muscle tissue engineering.," Biomaterials, **26**(22), pp. 4606–15.

[54] Radisic M., Euloth M., Yang L., Langer R., Freed L. E., and Vunjak-Novakovic G., 2003, "High-density seeding of myocyte cells for cardiac tissue engineering." Biotechnology and bioengineering, **82**(4), pp. 403–14.

[55] Thompson O., Moore C. J., Hussain S.-A., Kleino I., Peckham M., Hohenester E., Ayscough K. R., Saksela K., and Winder S. J., 2010, "Modulation of cell spreading and cell-substrate adhesion dynamics by dystroglycan.," Journal of cell science, **123**(Pt 1), pp. 118–27.

[56] Lovett D. B., Shekhar N., Nickerson J. a., Roux K. J., and Lele T. P., 2013, "Modulation of Nuclear Shape by Substrate Rigidity," Cellular and Molecular Bioengineering.

[57] Dou Y., Arlock P., and Arner A., 2007, "Blebbistatin specifically inhibits actin-myosin interaction in mouse cardiac muscle.," American journal of physiology. Cell physiology, **293**(3), pp. C1148–53.

[58] Kovács M., Tóth J., Hetényi C., Málnási-Csizmadia A., and Sellers J. R., 2004, "Mechanism of blebbistatin inhibition of myosin II.," The Journal of biological chemistry, **279**(34), pp. 35557–63.

[59] Raab M., Swift J., P. Dingal P. C. D., Shah P., Shin J.-W., and Discher D. E., 2012, "Crawling from soft to stiff matrix polarizes the cytoskeleton and phosphoregulates myosin-II heavy chain," The Journal of Cell Biology, **199**(4), pp. 669–683.

[60] Chang S. S., Guo W.-H., Kim Y., and Wang Y.-L., 2013, "Guidance of cell migration by substrate dimension.," Biophysical journal, **104**(2), pp. 313–21.

[61] Turner C. E., 1998, "Molecules in focus Paxillin," The International Journal of Biochemistry & Cell Biology, **30**(9), pp. 955–959.

[62] Aubin H., Nichol J. W., Hutson C. B., Bae H., Sieminski A. L., Cropek D. M., Akhyari P., and Khademhosseini A., 2010, "Directed 3D cell alignment and elongation in microengineered hydrogels.," Biomaterials, **31**(27), pp. 6941–6951.

[63] Kim D.-H., and Wirtz D., 2012, "Focal adhesion size uniquely predicts cell migration.," FASEB journal : official publication of the Federation of American Societies for Experimental Biology, pp. 1–11.

[64] Li Z., Song J., Mantini G., Lu M., Fang H., Falconi C., Chen L., and Wang Z. L., 2009, "Quantifying the Traction Force of a Single Cell by Aligned Silicon Nanowire Array," Nano.

[65] Pelham R. J., and Wang Y. L., 1998, "Cell locomotion and focal adhesions are regulated by the mechanical properties of the substrate.," The Biological bulletin, **194**(3), pp. 348–9; discussion 349–50.

[66] Sanz-Herrera J. a, Moreo P., García-Aznar J. M., and Doblaré M., 2009, "On the effect of substrate curvature on cell mechanics.," Biomaterials, **30**(34), pp. 6674–86.

[67] Lee S. J., and Yang S., 2012, "Micro glass ball embedded gels to study cell mechanobiological responses to substrate curvatures.," The Review of scientific instruments, **83**(9), p. 094302.

[68] Yeung T., Georges P. C., Flanagan L. a, Marg B., Ortiz M., Funaki M., Zahir N., Ming W., Weaver V., and Janmey P. a, 2005, "Effects of substrate stiffness on cell morphology, cytoskeletal structure, and adhesion.," Cell motility and the cytoskeleton, **60**(1), pp. 24–34.

[69] Kim D.-H., and Wirtz D., 2012, "Focal adhesion size uniquely predicts cell migration.," FASEB journal : official publication of the Federation of American Societies for Experimental Biology, pp. 1–11.

[70] Ghosh K., Pan Z., Guan E., Ge S., Liu Y., Nakamura T., Ren X.-D., Rafailovich M., and Clark R. a F., 2007, "Cell adaptation to a physiologically relevant ECM mimic with different viscoelastic properties.," Biomaterials, **28**(4), pp. 671–9.

[71] Thompson O., Moore C. J., Hussain S.-A., Kleino I., Peckham M., Hohenester E., Ayscough K. R., Saksela K., and Winder S. J., 2010, "Modulation of cell spreading and cell-substrate adhesion dynamics by dystroglycan," Journal of cell science, **123**(Pt 1), pp. 118–27.

[72] Han S. J., Bielawski K. S., Ting L. H., Rodriguez M. L., and Sniadecki N. J., 2012, "Decoupling substrate stiffness, spread area, and micropost density: a close spatial relationship between traction forces and focal adhesions.," Biophysical journal, **103**(4), pp. 640–8.

[73] Kuo C.-H. R., Xian J., Brenton J. D., Franze K., and Sivaniah E., 2012, "Complex Stiffness Gradient Substrates for Studying Mechanotactic Cell Migration.," Advanced materials (Deerfield Beach, Fla.), pp. 6059–6064.

[74] Gray D. S., Tien J., and Chen C. S., 2002, "Repositioning of cells by mechanotaxis on surfaces with micropatterned Young ' s modulus."

[75] Engler A. J., Sen S., Sweeney H. L., and Discher D. E., 2006, "Matrix elasticity directs stem cell lineage specification.," Cell, **126**(4), pp. 677–89.

[76] Ulrich T. a, De Juan Pardo E. M., and Kumar S., 2009, "The mechanical rigidity of the extracellular matrix regulates the structure, motility, and proliferation of glioma cells.," Cancer research, **69**(10), pp. 4167–74.

[77] Kim D.-H., and Wirtz D., 2012, "Focal adhesion size uniquely predicts cell migration.," FASEB journal : official publication of the Federation of American Societies for Experimental Biology, pp. 1–11.

[78] Budynas R. G., Nisbett K. J., and Shigley J. E., 2011, Shigley's Mechanical Engineering Design, McGraw-Hill, New York, NY.

[79] Peeters E. a G., Oomens C. W. J., Bouten C. V. C., Bader D. L., and Baaijens F. P. T., 2005, "Mechanical and failure properties of single attached cells under compression.," Journal of biomechanics, **38**(8), pp. 1685–93.

[80] Trickey W. R., Baaijens F. P. T., Laursen T. a, Alexopoulos L. G., and Guilak F., 2006, "Determination of the Poisson's ratio of the cell: recovery properties of chondrocytes after release from complete micropipette aspiration.," Journal of biomechanics, **39**(1), pp. 78–87.

[81] Tan J. L., Tien J., Pirone D. M., Gray D. S., Bhadriraju K., and Chen C. S., 2003, "Cells lying on a bed of microneedles: an approach to isolate mechanical force.," Proceedings of the National Academy of Sciences of the United States of America, **100**(4), pp. 1484–9.

[82] Burton K., Park J. H., and Taylor D. L., 1999, "Keratocytes generate traction forces in two phases.," Molecular biology of the cell, **10**(11), pp. 3745–69.

Appendix A: AFM Structural Stiffness Testing

A.1 Representative Deflection Data

μm	nm
0.000	-41.143
0.007	-41.033
0.014	-40.923
0.021	-40.786
0.029	-40.676
0.036	-40.539
0.043	-40.401
0.050	-40.291
0.057	-40.127
0.064	-40.017
0.071	-39.879
0.078	-39.769
0.086	-39.632
0.093	-39.522
0.100	-39.385
0.107	-39.248
0.114	-39.110
0.121	-39.000
0.128	-38.863
0.135	-38.753
0.143	-38.616
0.150	-38.506
0.157	-38.369
0.164	-38.259
0.171	-38.149
0.178	-38.012
0.185	-37.874
0.192	-37.765
0.200	-37.627
0.207	-37.490
0.214	-37.353
0.221	-37.243
0.228	-37.105
0.235	-36.968
0.242	-36.831
0.249	-36.721
0.257	-36.584
0.264	-36.446

A.2 Methods for Finding Fiber Force and Deflection Curves

Fiber structural stiffness testing was conducted using a Veeco Bioscope II AFM. The AFM was used in ramp testing mode. First, a tipless cantilever (App Nano) was loaded into the AFM, calibrated, and thermal tuning was performed to find the exact spring constant of the cantilever. Thermal tuning has been shown to be acceptably accurate for determination of cantilever spring constant, with 5 to 10% uncertainty dependent on parameters entered [51]. Cantilever spring constant was calibrated to a value within the manufacturer's listed specifications.

When cantilever spring constant was determined and entered into the AFM interface, a single fiber on a sample was found optically, and then the cantilever was brought into contact with the fiber. After making contact with the fiber, the AFM was set to ramp mode, and the fiber was deflected a set amount (3.642 µm). When a steady state deflection curve was obtained, values of cantilever deflection and total ramp distance were output to a text file and saved. Representative text files can be seen in Appendix A.1.

When text files showing ramp movement and deflection were obtained, a custom Matlab program was used to find force applied by the cantilever to the fiber and the subsequent fiber deflection. The equations used to find these values can be found in Appendix A.2. After the force applied and subsequent fiber deflection was found, these values were plotted. The slope of the line that describes the relationship between these parameters is the equivalent fiber structural stiffness at that point.

66

This technique was used to characterize fiber stiffness at several points along a single fiber, allowing for semi-complete characterization of the gradient of stiffness that occurs along the fiber.

A.3 Description of Structural Stiffness Calculation

In order to find the fiber structural stiffness, data output from the AFM needs to be manipulated in several ways. The AFM produced data files that showed the cantilever base ramp movement and the resulting cantilever deflection. From these values two parameters were found, force applied to the fiber and fiber deflection. Force was found using Equation A. 1.

$$Force = k_{cant}\delta_{cant}$$

Equation A. 1

Where k_{cant} is the spring constant of the cantilever, found using the thermal tune method and δ_{cant} is the deflection of the cantilever. This gives the force applied by the cantilever at each measurement of base movement. Then, the fiber deflection can be found by using Equation A. 2

$$\delta_{fiber} = \delta_{base} - \delta_{cant}$$

Equation A. 2

Where δ_{base} is the movement of the cantilever base, δ_{cant} is the cantilever deflection, and δ_{fiber} is the resulting fiber deflection. This gives a value of fiber deflection for each measurement of base movement. This parameter along with the force applied is then plotted to show the force-deflection curve of the fiber at this point. A line is fit to the curve, and the slope of the fit line is the structural stiffness at that point. Representative curves showing force deflection curves for the same fiber at the center and near the fixed end can be seen in Figure A. 1.
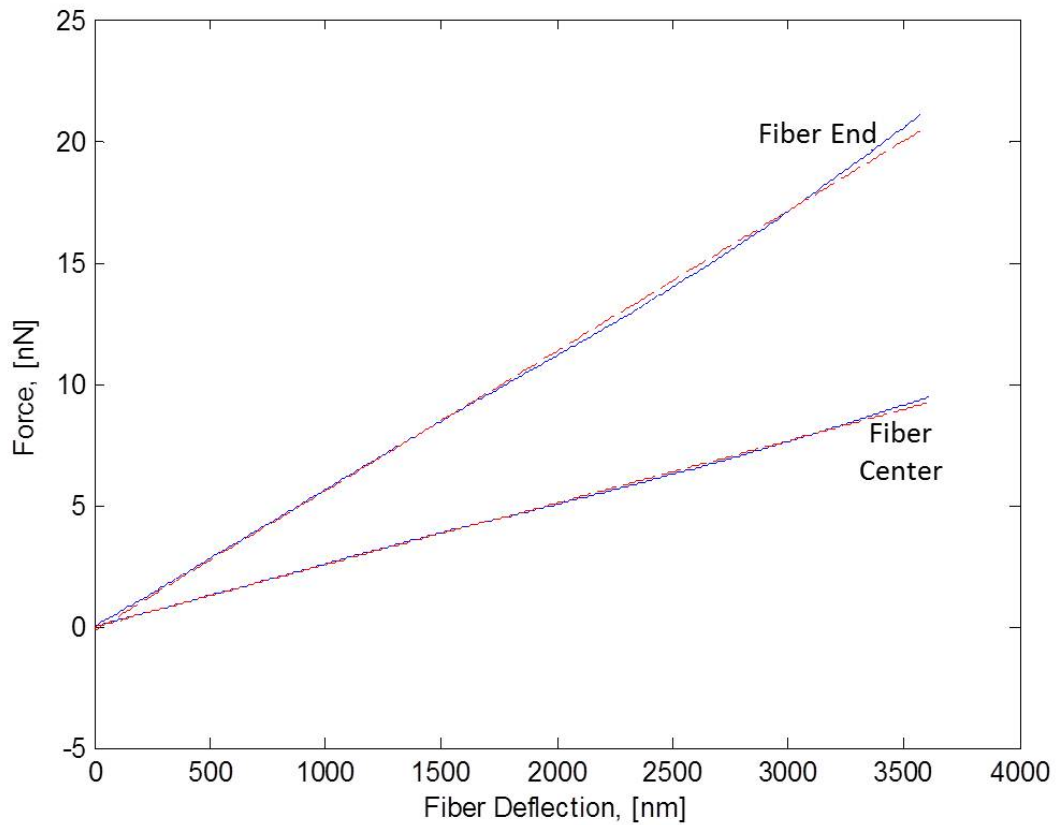
Figure A. 1. Force deflection curves for a single fiber near the center and near the fixed end. The difference in slope corresponding to a higher structural stiffness can be clearly seen.

A.4 Structural Stiffness Gradient Curves

Structural stiffness was characterized by AFM for several fiber configurations. Figure A.

2 shows several curves depicting structural stiffness along different configurations.
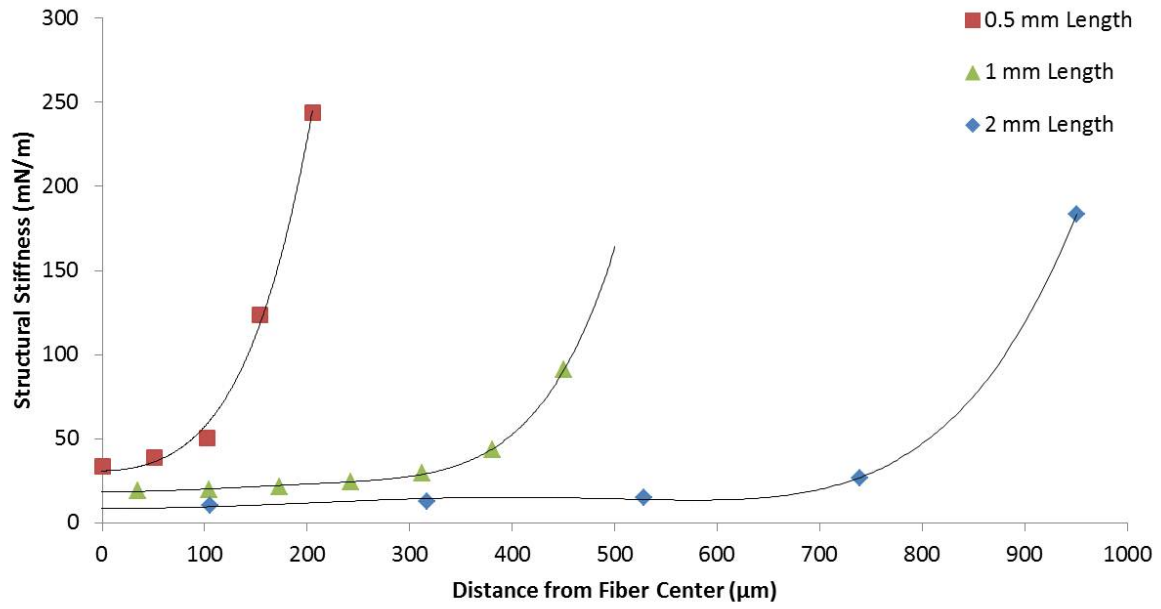
Figure A. 2. Measured structural stiffness values for three different lengths of 700 nm suspended fibers. Similar trends can be seen in all three cases.

Appendix B: Hertz Contact Mechanics: Single Cell on Fiber

B.1 Contact Mechanics Model: Cylinder-Cylinder Contact

To provide an estimate value of focal adhesion area, cell spreading was estimated using Hertz contact mechanics. Cells spreading around fibers were modeled as a cylinder-cylinder interaction [78]. Young's modulus for a cell was estimated as 1 kPa [79], and the material Young's modulus of PS estimated as 3 GPa. The Poisson ratio of the cell was estimated as 0.3[80], and the Poisson ratio used for the fiber was the commonly accepted value for polymers (0.5). Using these values, the degree of wrapping of the cell around the fiber that would result from normal adhesion forces (17 nN) [81,82]. The amount of wrapping found using these methods can be seen in Table B. 1

Table B. 1. Degree of Wrapping

Fiber Diameter (nm)	400	700	1200
Fiber Circumference (µm)	1.257	2.199	3.769
Wrapping Circumference (µm)	0.864	1.135	1.469
Percentage of Fiber Wrapped	68.7%	51.6%	38.6%

These estimated cell wrapping amounts were used to estimate the focal adhesion area in Section 4.7.3.